Vol 441|15 June 2006|doi:10.1038/nature04724

nature

LETTERS

Suppression of basal autophagy in neural cells causes neurodegenerative disease in mice

Taichi Hara[1], Kenji Nakamura[2], Makoto Matsui[1,3,4], Akitsugu Yamamoto[5], Yohko Nakahara[2], Rika Suzuki-Migishima[2], Minesuke Yokoyama[6], Kenji Mishima[7], Ichiro Saito[7], Hideyuki Okano[8,9] & Noboru Mizushima[1,10]

Autophagy is an intracellular bulk degradation process through which a portion of the cytoplasm is delivered to lysosomes to be degraded[1–4]. Although the primary role of autophagy in many organisms is in adaptation to starvation, autophagy is also thought to be important for normal turnover of cytoplasmic contents, particularly in quiescent cells such as neurons. Autophagy may have a protective role against the development of a number of neurodegenerative diseases[5–8]. Here we report that loss of autophagy causes neurodegeneration even in the absence of any disease-associated mutant proteins. Mice deficient for *Atg5* (autophagy-related 5) specifically in neural cells develop progressive deficits in motor function that are accompanied by the accumulation of cytoplasmic inclusion bodies in neurons. In $Atg5^{-/-}$ cells, diffuse, abnormal intracellular proteins accumulate, and then form aggregates and inclusions. These results suggest that the continuous clearance of diffuse cytosolic proteins through basal autophagy is important for preventing the accumulation of abnormal proteins, which can disrupt neural function and ultimately lead to neurodegeneration.

Every eukaryotic cell has two main systems for the degradation of intracellular components: the ubiquitin–proteasome system and autophagy. Autophagy is a generic term for the degradation of cellular components in lysosomes[1–4]. Macroautophagy (hereafter referred to as autophagy) is believed to be the main pathway among several subtypes of autophagy. During the process of autophagy, small portions of cytoplasm are sequestered by autophagosomes and then degraded on fusion with lysosomes. In contrast to the ubiquitin–proteasome system, which accounts for most of the selective intracellular protein degradation, autophagy is less selective. Autophagy induced by starvation is a mechanism for producing amino acids within cells. In yeast, autophagy-defective cells are susceptible to starvation. In comparison, mice deficient for Atg5 and Atg7, which are essential for autophagosome formation[9], suffer from severe nutrient- and energy-insufficiency soon after birth[10,11]. Thus, adaptation to starvation is an evolutionarily conserved role of autophagy.

In addition to induced autophagy, a low level of constitutive autophagy is important for intracellular clearance under normal conditions. Mice bearing a liver-specific conditional knockout allele of *Atg7* show hepatic dysfunction and intracellular ubiquitin-positive inclusion bodies[11]. We have also observed the accumulation of ubiquitin-positive inclusion bodies in hepatocytes and a subset of neurons in *Atg5*-knockout ($Atg5^{-/-}$) neonates (Supplementary Fig. S1); however, conventional histological analysis revealed no significant abnormality[10]. These data suggest that intracellular protein quality-control by autophagy is particularly important in neural cells. Indeed, several studies have suggested that impairment of autophagy could worsen the accumulation of abnormal proteins in neurodegenerative disease models *in vitro* and *in vivo*[5–8]. However, direct evidence demonstrating that autophagy contributes to the prevention of neurodegeneration has been lacking, in part because $Atg5^{-/-}$ and $Atg7^{-/-}$ mice die soon after birth[10,11].

To determine the role of autophagy in neural cells, we generated neural-cell-specific $Atg5^{-/-}$ mice (Supplementary Fig. S2). Mice bearing an $Atg5^{flox}$ allele, in which exon 3 of the *Atg5* gene is flanked by two *loxP* sequences, were crossed with a transgenic line expressing Cre recombinase under the control of the nestin promoter (nestin-*Cre*)[12]. In these mice, Cre recombinase is expressed in neural precursor cells after embryonic day (E)10.5, causing deletion of the *loxP*-flanked exon 3 (Supplementary Fig. S3). Recombination was successful in over 90% of all brain cells from $Atg5^{flox/flox}$; nestin-*Cre* mice. The expression of Atg5 (detected as an Atg12–Atg5 conjugate[13]) and the Atg5-dependent conversion of microtubule-associated protein 1 light chain 3 (LC3)-I to LC3-II (LC3–phosphatidylethanolamine (LC3–PE) conjugate)[13,14] were almost completely suppressed in the brains of $Atg5^{flox/flox}$; nestin-*Cre* mice after E15.5 (Fig. 1a and Supplementary Fig. S3). These data suggest that autophagosome formation is impaired in the brains of these mutant mice.

$Atg5^{flox/flox}$; nestin-*Cre* mice were born normally and survived neonatal starvation. They did not show the suckling defects observed in $Atg5^{-/-}$ and $Atg7^{-/-}$ neonates[10,11], suggesting that an undetectable, but sufficient, level of Atg5 remains in the neurons controlling the suckling response at this stage, or that non-neural cells may mediate the suckling deficit in the non-conditional mutants. However, the $Atg5^{flox/flox}$; nestin-*Cre* mice showed growth retardation: their mean body weight was about 1.5-times lower than that of control ($Atg5^{flox/+}$; nestin-*Cre*) mice (Fig. 1b). $Atg5^{flox/flox}$; nestin-*Cre* mice developed progressive motor and behavioural deficits after three weeks of age, and footprint analysis revealed an ataxic walking pattern (Fig. 1c). Mean stride lengths corrected for paw base widths were significantly decreased compared with control ($Atg5^{flox/+}$; nestin-*Cre*) mice. The $Atg5^{flox/flox}$; nestin-*Cre* mice showed limb-clasping reflexes when they were suspended by their tails, whereas control mice extended their limbs (Fig. 1d). This abnormal reflex is often observed in mouse models of neurodegenerative disease[15,16].

[1]Department of Bioregulation and Metabolism, Tokyo Metropolitan Institute of Medical Science, Tokyo 113-8613, Japan. [2]Mouse Genome Technology Laboratory, Mitsubishi Kagaku Institute of Life Sciences, Tokyo 194-8511, Japan. [3]Department of Basic Biology, School of Life Science, the Graduate University for Advanced Studies, Okazaki 444-8585, Japan. [4]Department of Cell Biology, National Institute for Basic Biology, Okazaki 444-8585, Japan. [5]Department of Bio-Science, Nagahama Institute of Bio-Science and Technology, Nagahama 526-0829, Japan. [6]Brain Research Institute, Niigata University, Niigata 951-8510, Japan. [7]Department of Pathology, Tsurumi University School of Dental Medicine, Yokohama 230-8501, Japan. [8]Department of Physiology, Keio University School of Medicine, Tokyo 160-8582, Japan. [9]SORST and [10]PRESTO, Japan Science and Technology Agency, Kawaguchi 332-0012, Japan.

Rotarod (Fig. 1e) and wire-hanging (data not shown) tasks also showed severely impaired motor coordination, balance and grip strength in *Atg5*$^{flox/flox}$; nestin-*Cre* mice. Finally, tremor was apparent in 12-week-old mice. Some of the *Atg5*$^{flox/flox}$; nestin-*Cre* mice died after three weeks of age. Neither *Atg5*$^{flox/flox}$ mice (Cre-negative) nor *Atg5*$^{flox/+}$; nestin-*Cre* mice showed any abnormal phenotype.

The gross anatomy of the brain of the mutant mice was normal. However, histological examination revealed degenerative changes in the neurons of *Atg5*$^{flox/flox}$; nestin-*Cre* mice. These alterations were most prominent in cerebellar Purkinje cells. Haematoxylin and eosin (H&E) staining (arrowheads in Fig. 2a) and immunohistochemical staining with an antibody directed against calbindin (a selective marker for Purkinje cells, left panels in Fig. 2b), demonstrated partial loss of these neurons (Fig. 2c). The remaining Purkinje cells showed eccentrically located nuclei, with infolding of the nuclear membrane. We also found a number of eosinophilic spheroids in H&E-stained sections in the cerebellar nuclei of these mutant mice (arrows in Fig. 2a), which probably correspond to the calbindin-positive spheroids in the same region (Fig. 2b, right panels). These structures suggest massive swelling of Purkinje cell axons that project to the cerebellar nuclei[17,18]. In addition, TUNEL-positive cells were detected in the adjacent granular layer, suggesting apoptosis of granular cells in *Atg5*$^{flox/flox}$; nestin-*Cre* mice (Fig. 2d). Consistent with previous observations, the survival of granular cells largely depends on their synaptic connectivity with Purkinje cells[19]. Axonal swelling was observed in other regions of the *Atg5*$^{flox/flox}$; nestin-*Cre* brain, including the cerebral cortex, the nucleus gracilis (Fig. 2a), the posterior thalamic nucleus, hippocampus, inferior colliculus, trigeminal nucleus, parabranchial nucleus, anterior thalamic nucleus, caudal pons and reticular nucleus (data not shown). Partial loss of pyramidal cells also was observed in the cerebral cortex (data not shown). Together, these data suggest that *Atg5*$^{flox/flox}$; nestin-*Cre* mice suffer from neurodegeneration.

We next examined protein aggregation in the brain using an antibody against ubiquitin, a marker of misfolded proteins. Large, ubiquitin-positive inclusion bodies accumulated in the cytoplasm of large neurons in the thalamus, pons, medulla, dorsal root ganglion (DRG) (Fig. 3a) and midbrain (data not shown) of *Atg5*$^{flox/flox}$; nestin-*Cre* mice. Neurons in the cerebral cortex, hippocampus (especially in the CA3 and CA4 regions) (Fig. 3a), striatum and olfactory bulb (data not shown) were also positive for these inclusion

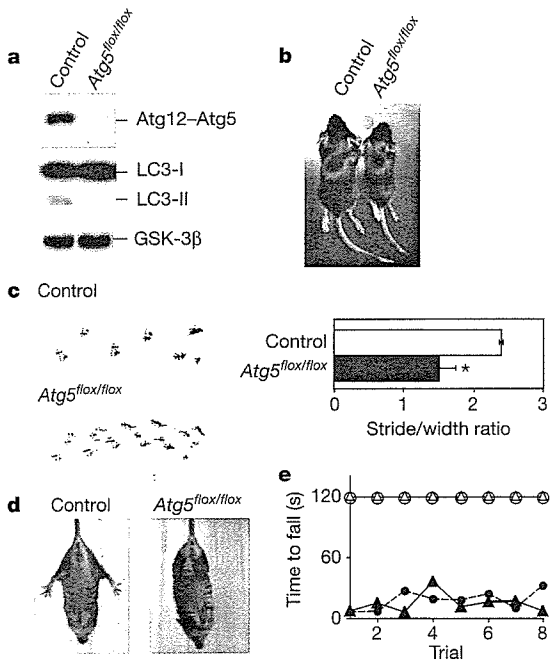

Figure 1 | Behavioural abnormalities in mice lacking *Atg5* in the nervous system. **a**, Immunoblot analysis of Atg5 and LC3. Brain homogenates were prepared from six-week-old control (*Atg5*$^{flox/+}$; nestin-*Cre*) and *Atg5*$^{flox/flox}$; nestin-*Cre* (*Atg5*$^{flox/flox}$) mice. Immunoblot analysis was performed using antibodies against Atg5 and LC3. GSK-3β was used as a loading control. The positions of the Atg12–Atg5 conjugate, LC3-I and LC3-II (LC3–PE conjugate) are indicated. Atg5 monomer was not detected in either lane (data not shown). **b**, A representative male control (*Atg5*$^{flox/+}$; nestin-*Cre*) and an *Atg5*$^{flox/flox}$; nestin-*Cre* (*Atg5*$^{flox/flox}$) littermate at three weeks of age. **c**, Left, paw placement records of eight-week-old mice. Right, stride lengths corrected for paw base widths (stride/width ratio) of *Atg5*$^{flox/flox}$; nestin-*Cre* and control (*Atg5*$^{flox/+}$; nestin-*Cre*) littermate mice. Values represent means ± s.d. of four mice. Asterisk, $P < 0.01$ (Student's *t*-test). **d**, Abnormal limb-clasping of an *Atg5*$^{flox/flox}$; nestin-*Cre* mouse compared with a control mouse (*Atg5*$^{flox/+}$; nestin-*Cre*) when suspended by its tail. **e**, Rotarod testing of *Atg5*$^{flox/+}$; nestin-*Cre* (open symbols) and *Atg5*$^{flox/flox}$; nestin-*Cre* (closed symbols) mice. One male and one female mouse were analysed for each genotype. The time until drop from the rod (rotating at 20 r.p.m.) is shown.

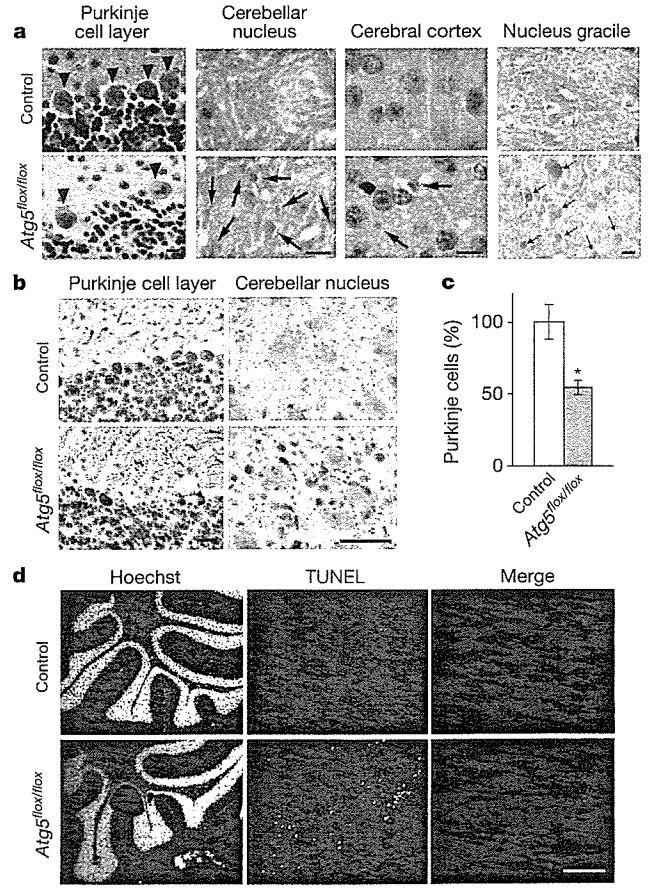

Figure 2 | Neuronal degeneration in *Atg5*$^{flox/flox}$; nestin-*Cre* mice. **a**, H&E-stained sections of the cerebral cortex, the gracile nucleus and cerebellum from control (*Atg5*$^{flox/+}$; nestin-*Cre*) and *Atg5*$^{flox/flox}$; nestin-*Cre* (*Atg5*$^{flox/flox}$) mice at three months of age. Purkinje cells are indicated with arrowheads. Arrows indicate eosinophilic spheroids, which represent axon swelling. Scale bar, 10 μm. **b**, Immunohistochemistry using an anti-calbindin antibody on cerebellum sections from control (*Atg5*$^{flox/+}$; nestin-*Cre*) and *Atg5*$^{flox/flox}$; nestin-*Cre* mice at six weeks of age. Scale bar, 25 μm. **c**, Loss of Purkinje cells in *Atg5*$^{flox/flox}$; nestin-*Cre* mice. Purkinje cells were counted in comparable areas for each mouse, and three fields were counted in each area for each mouse. Data are normalized against values from control mice (*Atg5*$^{flox/+}$; nestin-*Cre*). Values represent mean ± s.d. of three mice. Asterisk, $P < 0.01$ (*t*-test). **d**, Apoptotic death of granular cells. Cerebellum sections from control (*Atg5*$^{flox/+}$; nestin-*Cre*) and *Atg5*$^{flox/flox}$; nestin-*Cre* mice at six weeks of age were subjected to TUNEL staining. Nuclei were stained with Hoechst 33258. Scale bar, 500 μm.

bodies. Such inclusion bodies were not observed in the brains of control ($Atg5^{flox/+}$; nestin-*Cre*) mice. We observed ubiquitin-positive inclusion bodies exclusively in cells positive for the neural cell marker NeuN, suggesting that inclusion bodies were generated only in neurons and not in glial cells (Fig. 3b). Notably, although there was extensive loss of Purkinje cells, these neurons had very few inclusion bodies in their cell bodies (Fig. 3a). Numerous ubiquitin-positive dots were observed in the cerebellar nuclei (Fig. 3a), but most of them did not colocalize with the calbindin dots observed in Fig. 2b (data not shown).

The accumulation of inclusion bodies was time-dependent, and the distribution of inclusion-body-positive cells was more limited in $Atg5^{-/-}$ and $Atg5^{flox/flox}$; nestin-*Cre* newborns compared to adult mice. In $Atg5^{-/-}$ neonates, inclusion bodies were observed in the pons, DRG, spinal cord (ventral horn) (Supplementary Fig. S1), hypothalamus, midbrain and trigeminal ganglia (data not shown), but not in the cerebral cortex (Supplementary Fig. S1). A similar pattern was observed in the brain and DRG of $Atg5^{flox/flox}$; nestin-*Cre* neonates (Supplementary Fig. S4 and data not shown). Immuno-electron microscopy of DRG neurons isolated from $Atg5^{-/-}$ neonates

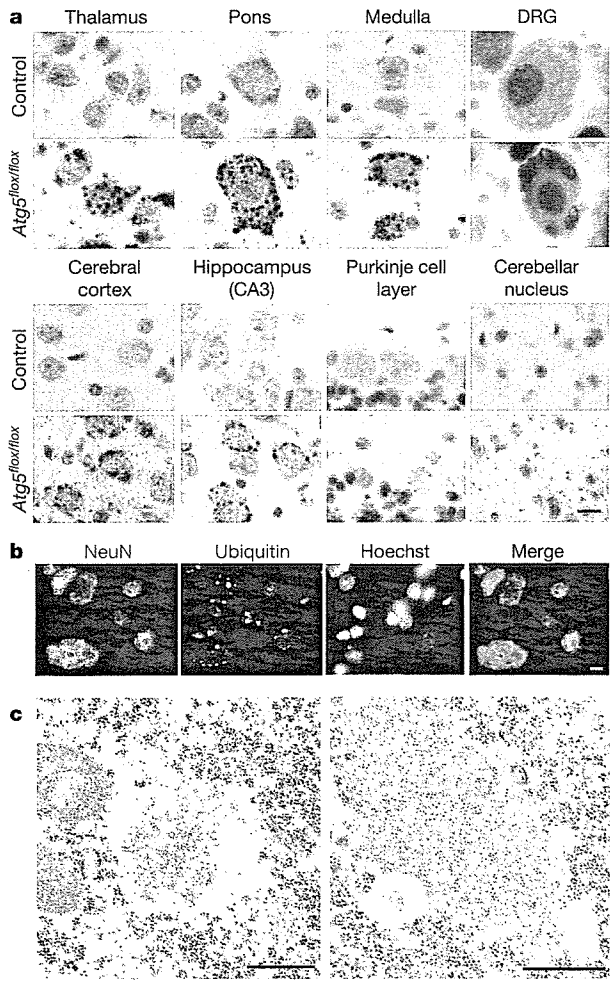

Figure 3 | Ubiquitin-positive inclusions in *Atg5*-deficient neurons. **a**, Immunohistochemistry of brain sections from control ($Atg5^{flox/+}$; nestin-*Cre*) and $Atg5^{flox/flox}$; nestin-*Cre* ($Atg5^{flox/flox}$) mice at six weeks of age, stained with an anti-ubiquitin antibody (1B3). Scale bar, 10 μm. **b**, Ubiquitin-positive inclusions in neurons. Sections of medulla from $Atg5^{flox/flox}$; nestin-*Cre* mice at six weeks of age were stained with an antibody against NeuN (a neuron-specific nuclear protein) and ubiquitin. Nuclei were stained with Hoechst 33258. Scale bar, 10 μm. **c**, Immunoelectron microscopy of ubiquitin-positive inclusion bodies. DRG neurons isolated from $Atg5^{-/-}$ neonates were analysed by immunoelectron microscopy using an anti-ubiquitin antibody. Scale bars, 500 nm.

demonstrated the specific association of ubiquitin with amorphous, occasionally filamentous, structures (Fig. 3c, left), as well as with more compact structures surrounded by filamentous materials (Fig. 3c, right; see Supplementary Fig. S5 for larger images). Outside the brain, $Atg5^{-/-}$ neonates showed inclusion body formation in the liver, the anterior lobe of pituitary gland (Supplementary Fig. S1) and the adrenal gland (data not shown).

Histological examination of $Atg5^{-/-}$ and $Atg5^{flox/flox}$; nestin-*Cre* mice suggested that, in addition to the presence of inclusion bodies, the intensity of diffuse cytoplasmic ubiquitin staining was higher compared with wild-type mice. We thus analysed the time course of accumulation of diffuse ubiquitinated proteins and inclusions in DRG neurons (the neonatal tissue in which inclusion body formation was most striking). DRG neurons from $Atg5^{-/-}$ embryos at E13.5 had no apparent abnormality. However, at E15.5, some neurons had accumulated diffuse, cytosolic ubiquitinated proteins with infrequent inclusions (Fig. 4a). Later, in newborn (postnatal day (P)0) $Atg5^{-/-}$ mice, multiple ubiquitin-positive inclusion bodies were present in DRG neurons. Thus, the accumulation of diffuse abnormal proteins seems to be the primary cellular phenotype of $Atg5^{flox/flox}$; nestin-*Cre* neurons. We obtained similar results using a biochemical method with whole brains. Polyubiquitinated proteins that accumulated in $Atg5^{flox/flox}$; nestin-*Cre* brains were primarily Triton-soluble in six-week-old mice (Fig. 4b). In contrast, in 14-week-old mice, Triton-insoluble polyubiquitinated proteins were also abundant, suggesting that inclusion body formation is a later event.

We confirmed these observations using hepatocytes, another cell type that showed extensive inclusion body accumulation under autophagy-defective conditions[11] (Supplementary Fig. S1). We crossed $Atg5^{flox/flox}$ mice with CAG-*Cre* mice that express Cre recombinase ubiquitously (see Methods)[20]. As recombination efficiency was not high when crossed with our $Atg5^{flox/flox}$ mice, the resulting mice ($Atg5^{flox/flox}$; CAG-*Cre*) were mosaic for the mutant allele and viable. In the livers of these mice, the *Atg5* gene was deleted in only about 30% of hepatocytes (Supplementary Fig. S6), which allowed us to compare directly the immunoreactivity of knockout cells with that of wild-type cells in the same specimen. Anti-ubiquitin staining of the liver in four-month-old $Atg5^{flox/flox}$; CAG-*Cre* mice showed that about 30% of cells had very high levels of diffuse cytoplasmic signals (in addition to inclusion bodies), compared with surrounding cells that were probably wild type (Fig. 4c). The results clearly demonstrate that cytosolic ubiquitinated proteins also accumulate in $Atg5^{-/-}$ hepatocytes.

We then determined the time course of accumulation of ubiquitinated proteins using Mx1-*Cre* transgenic mice[21]. In this system, Cre recombinase is expressed under the control of an interferon-responsive promoter that can be activated by application of polyinosinic acid-polycytidylic acid (pIpC), an interferon-inducible, synthetic double-stranded RNA. The *Atg5* gene in $Atg5^{flox/flox}$; Mx1-*Cre* liver was deleted by intraperitoneal injection of pIpC. Soon after injection, most targeted cells showed only diffuse ubiquitin staining, with no inclusion bodies (Fig. 4d, e). In contrast, large, ubiquitin-positive inclusion bodies were present in almost all targeted hepatocytes 16 days after pIpC injection (arrowheads in Fig. 4d). Cells with only inclusion bodies but not diffuse cytoplasmic staining were observed very rarely. Taken together, our data demonstrate that loss of autophagy first leads to accumulation of diffuse abnormal proteins, followed by generation of inclusion bodies.

We have shown that the inhibition of autophagy in neural cells causes neurodegeneration and symptoms of neurological pathology. As the mouse model we used does not express any disease-associated mutant proteins, the phenotype of these mutant mice indicates that autophagy mediates essential and continuous turnover of intracellular proteins. This system is particularly important for neurons, in which deregulation of this degradation process can induce cell dysfunction. The role of autophagy could be even more critical if

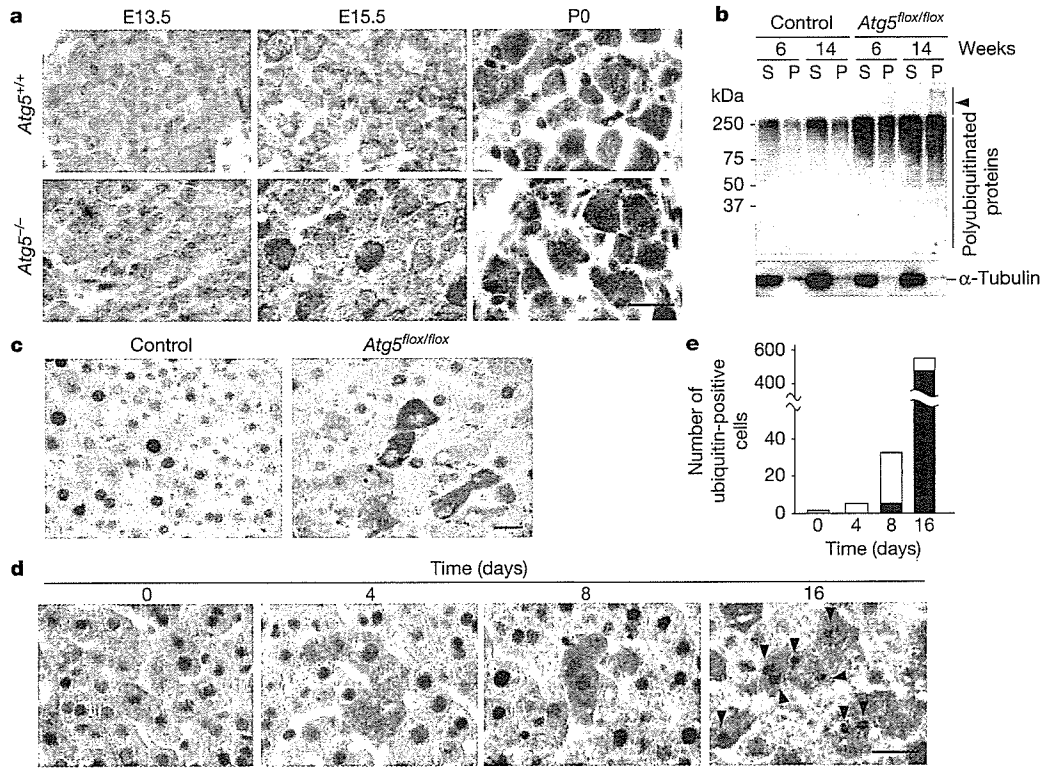

Figure 4 | Accumulation of diffuse ubiquitinated proteins in autophagy-defective cells. **a**, Immunohistochemistry of DRG neurons from $Atg5^{+/+}$ and $Atg5^{-/-}$ mice at different developmental stages (embryonic day (E)13.5, E15.5 or postnatal day (P)0), stained with an antibody directed against ubiquitin. Scale bar, 25 μm. **b**, Accumulation of Triton-X-100-soluble polyubiquitinated proteins in the brains of $Atg5^{flox/flox}$; nestin-*Cre* mice. Brain homogenate prepared at the indicated times from control ($Atg5^{flox/+}$; nestin-*Cre*) and $Atg5^{flox/flox}$; nestin-*Cre* ($Atg5^{flox/flox}$) mice were separated into Triton-X-100-soluble (S) and -insoluble (P) fractions and analysed by immunoblotting using anti-ubiquitin antibodies. Arrowhead indicates the stacking gel. **c**, Immunohistochemistry of liver sections from control ($Atg5^{flox/+}$; CAG-*Cre*) and $Atg5^{flox/flox}$; CAG-*Cre* ($Atg5^{flox/flox}$) mice at four months of age, using an anti-ubiquitin antibody. Scale bar, 25 μm. **d**, Immunohistochemistry of liver sections from six-week-old $Atg5^{flox/flox}$; Mx1-*Cre* mice at the indicated time points after pIpC injection, using anti-ubiquitin antibodies. Arrowheads indicate ubiquitin-positive inclusion bodies. Scale bar, 25 μm. **e**, Five thousand hepatocytes were randomly selected, and the number of cells with diffuse cytosolic ubiquitin signals, with (black) or without (white) inclusion bodies, were counted.

any aggregation-prone mutant proteins were expressed. Although autophagy is generally thought to be a non-selective process, several studies have suggested that autophagosomes can specifically engulf inclusion bodies[8,22]. In our system, however, inclusion bodies appeared in later phases of autophagy deficiency, suggesting that the primary role of autophagy under normal conditions is the turnover of diffuse cytosolic proteins, not direct elimination of inclusion bodies. As the population of ubiquitinated proteins in $Atg5^{flox/flox}$; nestin-*Cre* brains was similar to that in wild-type mouse brains, we suggest that cytoplasmic proteins that are usually ubiquitinated, rather than specific proteins, accumulate in larger amounts in the absence of autophagy (Supplementary Fig. S7). Downregulation of protein turnover could cause the accumulation of abnormal proteins, which then could promote aggregate formation (Supplementary Fig. S8).

The critical role of autophagy in the basal turnover of diffuse cytosolic proteins in neural cells should be emphasized, because it has been suggested that large inclusion bodies themselves might not be pathogenic, but that mutant proteins present diffusely in the cytosol could be the primary source of toxicity[23–27]. However, we do not rule out the possibility that autophagosomes can selectively recognize abnormal soluble proteins or microaggregates on the membrane surface. It was recently reported that the polyubiquitin-binding protein p62/SQSTM1 might mediate the specific recognition of protein aggregates by autophagosomes[28]. This pathway might also be involved in the degradation of diffuse ubiquitinated proteins by autophagy.

METHODS

Generation of tissue-specific *Atg5*-deficient mice. An approximately 1-kb *XbaI–SpeI* mouse genomic fragment containing putative exon 3 of the *Atg5* gene was flanked by two *loxP* sites containing the neomycin-resistant (*neo*^{r}) cassette from pMC1-Neo (Stratagene). The diphtheria toxin A (*DT-A*) gene was inserted downstream of the short arm, for negative selection against random integration of the vector (Supplementary Fig. S2). Targeted CCE embryonic stem cells of 129/SvEv mouse origin were injected into C57BL/6 blastocysts, and chimaeric mice were crossed with C57BL/6 mice to obtain $Atg5^{flox/+}$ mice. We used the following primers to detect wild-type *Atg5* and $Atg5^{flox}$ alleles: A (exon3-1), 5′-GAATATGAAGGCACACCCCTGAAATG-3′; B (short2), 5′-GTACTGCATAATGGTTTAACTCTTGC-3′; C (check2), 5′-ACAACGTCGAG CACAGCTGCGCAAGG-3′; D (5L2), 5′-CAGGGAATGGTGTCTCCCAC-3′; E (cre1), 5′-AGGTTCGTTCACTCATGGA-3′; F (cre2), 5′-TCGACCAGTTT AGTTACCC-3′.

Southern blot analysis was performed using the probe shown in Supplementary Fig. S2 after digestion of genomic DNA with *Eco*RV and *Kpn*I, as described previously[13]. Nestin-*Cre* transgenic mice expressing Cre recombinase under the control of the mouse nestin gene promoter and second intronic neural enhancer (a gift from S. Noguchi) have been described previously[29]. CAG-*Cre* transgenic mice expressing Cre recombinase under the control of the CAG (CMV enhancer and chicken β-actin) promoter have been described previously[20]. Mx1-*Cre* transgenic mice were obtained from the Jackson Laboratory[21]. Progeny containing the $Atg5^{flox}$ allele were bred with these *Cre* transgenic mice to generate $Atg5^{flox/flox}$; nestin-*Cre*, $Atg5^{flox/flox}$; CAG-*Cre* and $Atg5^{flox/flox}$; Mx1-*Cre* mice. $Atg5^{-/-}$ mice have been described previously[10]. All animal experiments were approved by the institutional committee of the Tokyo Metropolitan Institute of Medical Science.

Antibodies. A monoclonal antibody against ubiquitin (1B3) was purchased from

MBL and used for immunohistochemistry. Rabbit anti-ubiquitin polyclonal antibody (DakoCytomation) was used for immunoelectron microscopy. Anti-polyubiquitin monoclonal antibody (FK2, Nippon Bio-Test Laboratories) was used in immunoblot analyses. The following antibodies were also used: anti-NeuN monoclonal antibody (Chemicon), rabbit anti-calbindin polyclonal antibody (Chemicon), Alexa Fluor 488- and 660-conjugated goat anti-rabbit IgG (H + L) antibodies (Molecular Probes), monoclonal anti-glycogen synthase kinase-3β antibody (BD Biosciences), monoclonal anti-α-tubulin antibody (DM1A, Sigma-Aldrich), and antibodies against Atg5 (SO4)[13] and LC3[14].

Behavioural analysis. Mice were placed on a rod rotating at 20 r.p.m., and the time taken for them to fall from the rod was measured. If a mouse stayed on the rod until the end of the 2-min trial, a time of 120 s was recorded.

Immunohistochemical analysis. Mice were transcardially perfused with 4% paraformaldehyde in phosphate buffer (pH 7.4). Tissues were post-fixed in the same fixative overnight and embedded in paraffin. Sections were stained using Meyer's H&E. For immunohistochemical analysis, all tissue sections were subjected to antigen retrieval using the microwave method (in 0.01 M citrate buffer for 10 min). After blocking, sections were incubated with primary antibodies for 1 h, followed by 30 min incubation with fluorescently labelled or biotinylated secondary antibodies that were detected using Histomouse-plus kits (Zymed Laboratories) and the Liquid DAB substrate chromogen system (DakoCytomation). Apoptotic cells were detected by TUNEL assay using an *in situ* cell death detection kit (Roche Diagnostic).

Immunoelectron microscopy. For immunoelectron microscopy, the post-embedding immuno-gold method was used to label tissue sections embedded with LR white resin (London Resin Co.) as previously described[30].

Preparation of detergent-soluble and -insoluble fractions. Mouse brains were homogenized in five volumes of ice-cold 0.25 M sucrose buffer (50 mM Tris-HCl pH 7.4, 1 mM EDTA) with protease inhibitors. Homogenates were centrifuged at 500*g* for 10 min at 4 °C, and the resulting supernatants were lysed with an equal volume of cold sucrose buffer containing 1% Triton X-100. Lysates were subjected to centrifugation at 13,000*g* for 15 min at 4 °C to separate supernatants (fractions soluble in 0.5% Triton-X-100) and pellets. Pellets were resuspended in 1% SDS in PBS (Triton-X-100-insoluble fractions).

Received 6 February; accepted 20 March 2006.
Published online 19 April 2006.

1. Cuervo, A. M. Autophagy: in sickness and in health. *Trends Cell Biol.* **14**, 70–77 (2004).
2. Levine, B. & Klionsky, D. J. Development by self-digestion: molecular mechanisms and biological functions of autophagy. *Dev. Cell* **6**, 463–477 (2004).
3. Klionsky, D. J. The molecular machinery of autophagy: unanswered questions. *J. Cell Sci.* **118**, 7–18 (2005).
4. Mizushima, N. The pleiotropic role of autophagy: from protein metabolism to bactericide. *Cell Death Differ.* **12**, 1535–1541 (2005).
5. Ravikumar, B., Duden, R. & Rubinsztein, D. C. Aggregate-prone proteins with polyglutamine and polyalanine expansions are degraded by autophagy. *Hum. Mol. Genet.* **11**, 1107–1117 (2002).
6. Fortun, J., Dunn, W. A. Jr, Joy, S., Li, J. & Notterpek, L. Emerging role for autophagy in the removal of aggresomes in Schwann cells. *J. Neurosci.* **23**, 10672–10680 (2003).
7. Ravikumar, B. *et al.* Inhibition of mTOR induces autophagy and reduces toxicity of polyglutamine expansions in fly and mouse models of Huntington disease. *Nature Genet.* **36**, 585–595 (2004).
8. Iwata, A. *et al.* Increased susceptibility of cytoplasmic over nuclear polyglutamine aggregates to autophagic degradation. *Proc. Natl Acad. Sci. USA* **102**, 13135–13140 (2005).
9. Mizushima, N., Ohsumi, Y. & Yoshimori, T. Autophagosome formation in mammalian cells. *Cell Struct. Funct.* **27**, 421–429 (2002).
10. Kuma, A. *et al.* The role of autophagy during the early neonatal starvation period. *Nature* **432**, 1032–1036 (2004).
11. Komatsu, M. *et al.* Impairment of starvation-induced and constitutive autophagy in *Atg7*-deficient mice. *J. Cell Biol.* **169**, 425–434 (2005).
12. Betz, U. A., Vosshenrich, C. A., Rajewsky, K. & Muller, W. Bypass of lethality with mosaic mice generated by Cre–*loxP*-mediated recombination. *Curr. Biol.* **6**, 1307–1316 (1996).
13. Mizushima, N. *et al.* Dissection of autophagosome formation using Apg5-deficient mouse embryonic stem cells. *J. Cell Biol.* **152**, 657–667 (2001).
14. Kabeya, Y. *et al.* LC3, a mammalian homologue of yeast Apg8p, is localized in autophagosome membranes after processing. *EMBO J.* **19**, 5720–5728 (2000).
15. Cote, F., Collard, J. F. & Julien, J. P. Progressive neuronopathy in transgenic mice expressing the human neurofilament heavy gene: a mouse model of amyotrophic lateral sclerosis. *Cell* **73**, 35–46 (1993).
16. Mangiarini, L. *et al.* Exon 1 of the *HD* gene with an expanded CAG repeat is sufficient to cause a progressive neurological phenotype in transgenic mice. *Cell* **87**, 493–506 (1996).
17. Kikuchi, T., Mukoyama, M., Yamazaki, K. & Moriya, H. Axonal degeneration of ascending sensory neurons in gracile axonal dystrophy mutant mouse. *Acta Neuropathol. (Berl.)* **80**, 145–151 (1990).
18. Sotelo, C. Axonal abnormalities in cerebellar Purkinje cells of the 'hyperspiny Purkinje cell' mutant mouse. *J. Neurocytol.* **19**, 737–755 (1990).
19. Lossi, L., Mioletti, S. & Merighi, A. Synapse-independent and synapse-dependent apoptosis of cerebellar granule cells in postnatal rabbits occur at two subsequent but partly overlapping developmental stages. *Neuroscience* **112**, 509–523 (2002).
20. Sakai, K. & Miyazaki, J. A transgenic mouse line that retains Cre recombinase activity in mature oocytes irrespective of the *cre* transgene transmission. *Biochem. Biophys. Res. Commun.* **237**, 318–324 (1997).
21. Kuhn, R., Schwenk, F., Aguet, M. & Rajewsky, K. Inducible gene targeting in mice. *Science* **269**, 1427–1429 (1995).
22. Kopito, R. R. Aggresomes, inclusion bodies and protein aggregation. *Trends Cell Biol.* **10**, 524–530 (2000).
23. Saudou, F., Finkbeiner, S., Devys, D. & Greenberg, M. E. Huntingtin acts in the nucleus to induce apoptosis but death does not correlate with the formation of intranuclear inclusions. *Cell* **95**, 55–66 (1998).
24. Kuemmerle, S. *et al.* Huntington aggregates may not predict neuronal death in Huntington's disease. *Ann. Neurol.* **46**, 842–849 (1999).
25. Taylor, J. P. *et al.* Aggresomes protect cells by enhancing the degradation of toxic polyglutamine-containing protein. *Hum. Mol. Genet.* **12**, 749–757 (2003).
26. Arrasate, M., Mitra, S., Schweitzer, E. S., Segal, M. R. & Finkbeiner, S. Inclusion body formation reduces levels of mutant huntingtin and the risk of neuronal death. *Nature* **431**, 805–810 (2004).
27. Tanaka, M. *et al.* Aggresomes formed by α-synuclein and synphilin-1 are cytoprotective. *J. Biol. Chem.* **279**, 4625–4631 (2004).
28. Bjorkoy, G. *et al.* p62/SQSTM1 forms protein aggregates degraded by autophagy and has a protective effect on huntingtin-induced cell death. *J. Cell Biol.* **171**, 603–614 (2005).
29. Mori, H. *et al.* Socs3 deficiency in the brain elevates leptin sensitivity and confers resistance to diet-induced obesity. *Nature Med.* **10**, 739–743 (2004).
30. Yamamoto, A. *et al.* Stacks of flattened smooth endoplasmic reticulum highly enriched in inositol 1,4,5-trisphosphate ($InsP_3$) receptor in mouse cerebellar Purkinje cells. *Cell Struct. Funct.* **16**, 419–432 (1991).

Supplementary Information is linked to the online version of the paper at www.nature.com/nature. A summary figure is also included.

Acknowledgements We thank H. Neko, M. Miwa and Y. Kabeya for technical assistance. We also thank J. Miyazaki for the donation of CAG-*Cre* transgenic mice, T. Yoshimori for the anti-LC3 antibody, E. Yamada for histological examination, M. Yuzaki for the rotarod analysis, and A. Kuma for discussion. We thank Z. Yue for critical reading of the manuscript. This work was supported in part by Grants-in-Aid for Scientific Research from the Ministry of Education, Culture, Sports, Science and Technology of Japan. The authors thank the Yamada Science Foundation and the Cell Science Research Foundation for their financial support.

Author Contributions T.H. performed most of the experiments to characterize the neuron-specific knockout mice. M.M. analysed $Atg5^{-/-}$ mice. K.N., Y.N., R.S.-M. and M.Y. generated $Atg5^{flox}$ chimaeric mice. A.Y. performed electron microscopy. K.M. and I.S. performed histological analysis. H.O. provided nestin-*Cre* mice and participated in manuscript preparation. N.M. conceived the experiments and generated the targeting vector. T.H. and N.M. wrote the paper.

Author Information Reprints and permissions information is available at npg.nature.com/reprintsandpermissions. The authors declare no competing financial interests. Correspondence and requests for materials should be addressed to to N.M. (nmizu@rinshoken.or.jp).

Successful pregnancies after transplantation of frozen-thawed mouse ovaries into chimeric mice that received lethal-dose radiation

Fujio Migishima, M.D., Ph.D., Rika Suzuki-Migishima, B.A., Rudolfo B. Quintero, M.D., Minesuke Yokoyama, Ph.D., and Barry R. Behr, Ph.D., H.C.L.D.

Department of Neurobiology and Physiology, Northwestern University, Evanston, Illinois; Mitsubishi Kagaku Institute of Life Sciences, Tokyo, Japan; Brain Research Institute, Niigata University, Niigata, Japan; and Stanford University Medical Center, Stanford, California.

Reprinted from
FERTILITY AND STERILITY
Vol. 86, Suppl. 3, October 2006

Successful pregnancies after transplantation of frozen–thawed mouse ovaries into chimeric mice that received lethal-dose radiation

Fujio Migishima, M.D., Ph.D.,[a,d] *Rika Suzuki-Migishima, B.A.,*[b] *Rudolfo B. Quintero, M.D.,*[d] *Minesuke Yokoyama, Ph.D.,*[b,c] *and Barry R. Behr, Ph.D., H.C.L.D.*[d]

[a] Department of Neurobiology and Physiology, Northwestern University, Evanston, Illinois; [b] Mitsubishi Kagaku Institute of Life Sciences, Tokyo, Japan; [c] Brain Research Institute, Niigata University, Niigata, Japan; and [d] Stanford University Medical Center, Stanford, California

Objective: To study whether fecundity was recovered in mice into which umbilical cord blood cells (UCBCs) were transfused after lethal-dose radiation, followed by transplantation of frozen–thawed ovaries.
Design: Prospective basic research study.
Setting: Academic research laboratory.
Animal(s): Female C57BL/6 mice as recipients of UCBCs and ovaries, male B6C3F1 mice for mating, and green fluorescent protein (GFP)-transgenic mice: 18.5-day-old fetuses (−/+) for UCBCs and adult GFP mice (+/+) for ovarian tissues.
Intervention(s): The UCBCs were transfused into each irradiated mouse, with GFP+ ovaries transplanted 4 weeks later. The chimeric mice were mated 3 weeks after ovarian transplantation and were examined 14 to 16 weeks after the transfusion of UCBCs.
Main Outcome Measure(s): Percentage of chimerism, number of GFP+ pups.
Result(s): The percentage of chimerism in these mice tends to increase with the radiation dose. The recovery of fecundity was observed in the chimeric mice that were transplanted with fresh and previously vitrified ovaries after exposure to radiation.
Conclusion(s): Even when the exposure dose of radiation administered as pretreatment is lethal, the fecundity of recipients can be maintained if their ovaries are cryopreserved before they are exposed to radiation. (Fertil Steril® 2006;86(Suppl 3):1080–7. ©2006 by American Society for Reproductive Medicine.)

Key Words: Lethal-dose radiation, reconstitution of bone marrow function, umbilical cord blood, freezing and storing of ovaries, cryopreservation, transplantation of ovaries, pregnancy

The transfusion of hematopoietic stem cells is a possible treatment method for patients with inveterate blood diseases such as leukemia and severe anaplastic anemia.

However, it is known that pretreatments before hematopoietic stem cell transfusion, such as chemotherapy and irradiation, are harmful to gonadal functions and may lead to loss of fecundity (1–3). When these pretreatments are unavoidable, attempts to preserve future fecundity in willing patients should follow suit. One method of maintaining fecundity may be through ovarian cryopreservation (4). In particular, vitrification may be widely used in the future because of its ease of use.

In this study, female C57BL/6 mice were exposed to lethal-dose radiation, and then their bone marrow functions were restored by transfusion of murine umbilical cord blood cells (UCBCs). After the above processes, ovaries of green fluorescent protein (GFP)–transgenic C57BL/6TgN(act-EGFP)OsbY01 (GFP Y01) mice (+/+) (5), previously frozen and stored by vitrification, were transplanted to these radiation-exposed chimeric female mice; we then examined the recovery of fecundity in these female chimeric mice.

Received November 12, 2005; revised and accepted March 15, 2006.
Reprint requests: Fujio Migishima, M.D., Ph.D., Department of Neurobiology and Physiology, Northwestern University, 2205 Tech Drive, Hogan 4-150, Evanston, Illinois 60208 (FAX: 847-491-2224; E-mail: f-migishima@northwestern.edu).

MATERIALS AND METHODS

Animals

Female C57BL/6 and male GFP Y01 mice (+/+) were mated naturally. When successful mating was confirmed by the presence of a vaginal plug, the females were housed individually. The female C57BL/6 mice, recipients of UCBCs of radiation-chimeric mice, and male B6C3F1 mice were purchased from CLEA Japan Inc. (Tokyo, Japan). These mice were maintained at our animal facility under specific pathogen–free conditions. The mice were housed under a 12:12-hour light–dark cycle regimen at 22°C and 55% humidity. Food and water were freely available at all times.

All of the experiments using animals were in accordance with the International Guiding Principle for Biomedical Research Involving Animals. The experimental protocol was approved by the ethics committee for experimental animals of our facility.

0015-0282/06/$32.00
doi:10.1016/j.fertnstert.2006.03.023

Sampling of GFP+ Umbilical Cord Blood

Eighteen days after being confirmed by the presence of a vaginal plug, we used our method (6) of sampling mouse umbilical cord blood. Briefly, the uteri were removed from the pregnant females. After washing, they were cut into individual fetal lumps, the muscle layer of each uterus was removed, and fetuses with placenta covered with membranes were obtained. They were cooled in ice-cold phosphate-buffered saline, and the visceral yolk sac and amnion were removed. The cleaned fetuses with umbilical cord and placenta were immersed in warmed heparinized phosphate-buffered saline, prepared at 42°C that would drop the temperature to approximately 37°C after the cold fetus was immersed. Then the umbilical cord was cut, and blood was allowed to flow out until the fetus was completely pale. The collected blood in heparinized phosphate-buffered saline was processed by centrifuge. The supernatant was removed, and the precipitated whole blood was collected.

Preparation of Radiation-Chimeric Mice

Eight- to 10-week-old C57BL/6 female mice were irradiated with a roentgen irradiator (Hitachi Medico Co., Tokyo, Japan) with a filter (Cu: 0.5 mm, Al: 2 mm) monitoring the cumulative radiation dose. The mice received 8.0 Gy or 10 Gy of radiation. The obtained UCBCs, collected from the equivalent to two murine fetuses, then were transfused into each irradiated C57BL/6 mouse by IV injection. In this experiment, we used umbilical cord blood of GFP-transgenic mice (−/+) to clarify the percentage of GFP+ peripheral blood lymphocytes (PBLs) of chimeric mice and to conform the GFP+ lineages in PBLs of chimeric mice.

Frozen–Thawed Mouse Ovaries

We used our vitrification method for the frozen–thawed ovaries (4). Briefly, 8- to 12-week-old female homozygous GFP-transgenic mice were killed by cervical dislocation. Whole ovaries were aseptically removed and placed in 35- × 10-mm disposable Petri dishes (Becton Dickinson, Franklin Lakes, NJ) containing 3 mL of Whitten medium (7) kept at 0°C. Each of the isolated ovaries obtained was cut into two sections. The cut ovaries were soaked in the PBI medium (8) containing 1 M dimethyl sulfoxide at room temperature. Five microliters of the medium containing the two sections of ovaries then were transferred into a 1-mL cryotube (Nalge Nunc International KK, Tokyo, Japan), which then was placed in ice water for 5 minutes to allow dimethyl sulfoxide to thoroughly permeate the ovarian sections. Then, 95 μL of DAP 213 solution (9) maintained at 0°C was added to the cryotube. After the cryotubes were placed in ice water (0°C) for 5 minutes, they were immersed directly into liquid nitrogen and stored for 7 days. The samples were taken from the liquid nitrogen, allowed to stand at room temperature for 30 seconds, and later were diluted with 900 μL of PBI medium (37°C) containing 0.25 M sucrose. PBI medium was used afterwards for washing, with eventual transfer to Whitten's medium, both kept at 0°C.

Transplantation of Frozen–Thawed Ovaries to Radiation-Chimeric Mice

Four weeks after irradiation and transfusion of UCBCs, we orthotopically transplanted frozen–thawed ovaries from female homozygous GFP-transgenic mice to radiation-chimeric mice. Freshly isolated ovaries also were used in this experiment. We used our ovarian transplantation procedure (4). Briefly, radiation-chimeric mice were anesthetized with an IP injection of sodium pentobarbital (Dainippon Pharmaceutical Co., Ltd., Osaka, Japan), diluted at 1:10 (final concentration: 5 mg/mL) with isotonic sodium chloride solution (FUSO Pharmaceutical Industries Ltd., Osaka, Japan). A single median longitudinal skin incision was made on the lumbar portion to expose the subcutaneous tissue over the ovary. A small incision was made on the fascia and muscles immediately above the ovary, thereby exteriorizing the recipient's reproductive tract. One or two drops of 1:20 diluted epinephrine (final concentration: 50 mg/mL; Daiichi Pharmaceutical Co., Ltd., Tokyo, Japan) with isotonic sodium chloride solution were applied to the ovarian bursa to prevent bleeding. A small slit was made on the ovarian bursa to expose and remove both ovaries. A fresh or frozen–thawed half-ovary was inserted into one of the ovarian bursae of both sides. Then the reproductive tract was returned to the abdominal cavity. The skin incision was closed with clips (9-mm autoclips; Becton Dickinson).

Mating

The recipient female mice were allowed to recover for 3 weeks after the surgery and were then paired with male B6C3F1 mice. When successful mating was confirmed by the presence of a vaginal plug, the females were housed individually. If no vaginal plug was detected, pairing was continued for 8 weeks. The pups were observed under 360-nm ultraviolet light using a handheld illuminator (UltraViolet Products Ltd., Cambridge, Cambridgeshire, United Kingdom). Although GFP requires a blue light (488 nm) for excitation, its fluorescence is visible to the naked eye under ultraviolet light (5).

Flowcytometric Analysis of Cells From Chimeric Mice

Fourteen to 16 weeks after the irradiation of the chimeric mice and transfusion of UCBCs, the peripheral blood was obtained from the radiation-chimeric mice. The collected blood was processed by centrifuge on Lymphosepar II (specific gravity, 1.090; Immuno-Biological Laboratories, Fujioka, Japan) at 2,000 rpm for 20 minutes, and interface cells were collected. Approximately 10×10^5 cells were stained and washed with ice-cold Hanks' balanced salt solution containing 0.5% bovine serum albumin and 0.02% sodium azide. Secondary staining was performed in the same manner. T-cell receptor (CD3; T cells), B220 (CD45R; B cells), Mac-1 (CD11b; macrophages), Gr-1 (Ly-6G; granulocytes), or TER119 (Ly-76; erythroid cells were used in markers for staining), followed by PE streptavidin. Stained cells after washing were

examined by flow cytometry on FACSCalibur (Becton Dickinson, Mountain View, CA) to confirm the lineages and the percentage of GFP+ cells among PBLs of radiation-chimeric mice.

Histological Examination

Radiation-chimeric mice were killed 16 weeks after the transfusion of UCBCs. Their ovaries were removed and fixed in 4% (wt/vol) paraformaldehyde in 0.01 M phosphate buffer (PB, pH 7.2) at 4°C for 24 hours. After washing with 0.01 M PB, the ovaries were immersed for 24 hours in 7 % (wt/vol) sucrose in 0.01 M PB for cryoprotection. The ovaries were embedded in the OTC compound (Sakura Finetechnical Co., Ltd., Tokyo, Japan) and frozen at –70°C with dry ice and stored at −80°C until use. Frozen sections (8 μm thick) of the prepared ovaries were cut with a cryostat (Leica, Wetzlar, Germany). The sections were stained with a biotinylated anti-CD45 antibody, followed by staining with Texas Red–labeled streptavidin, and then they were observed under a fluorescence microscope (Leica).

Statistical Analysis

Values are expressed as mean ± SEM. Analysis of variance was performed, followed by multiple pairwise comparisons using the Tukey test. Significance was established as $P<.05$.

RESULTS

Flowcytometric Analysis of Chimeric Mice

Fourteen to 16 weeks after irradiation of chimeric mice and transfusion of UCBCs, peripheral blood was obtained from the radiation-chimeric mice. The obtained blood was processed by centrifuge, and cells on the interface were collected. The collected cells were subjected to flow cytometry to confirm the percentage of GFP+ cells among GFP+ PBLs of radiation-chimeric mice (Fig. 1), and it was confirmed that every lineage contained GFP+ cells (Fig. 2).

Table 1 summarizes the percentage of GFP+ cells among PBLs of the radiation-chimeric mice that were transplanted with no grafts or that were transplanted with fresh or frozen–thawed grafts. The percentage of GFP+ cells among PBLs circulating in chimeric mice that were exposed to 10.0 Gy radiation and transplanted with a frozen–thawed ovarian graft was significantly higher than that in mice that were exposed to 8.0 Gy radiation and transplanted with fresh ovaries. In addition, the percentages of GFP+ cells among PBLs of mice in the two groups that were exposed to 10.0 Gy radiation tended to be higher than those of mice in the two groups that were exposed to 8.0 Gy radiation. It is likely that with an increasing dose of radiation, the percentage of GFP+ cells among PBLs increases.

Fecundity of Radiation-Chimeric Mice

Four weeks after transfusion of UCBCs, we orthotopically engrafted fresh or frozen–thawed ovaries from female homozygous GFP-transgenic mice (+/+) to radiation-chimeric mice. The recipient female mice were allowed to recover for 3 weeks after the surgery and then were paired with male B6C3F1 mice. When successful mating was confirmed by the presence of a vaginal plug, the female radiation-chimeric mice were housed individually.

FIGURE 1

Flow-cytometric analysis of peripheral blood nucleated cells from C57BL/6 mice, GFP-transgenic mice, and radiation-chimeric mice transfused with GFP+ umbilical cord blood. *Bars*, GFP+ cells.

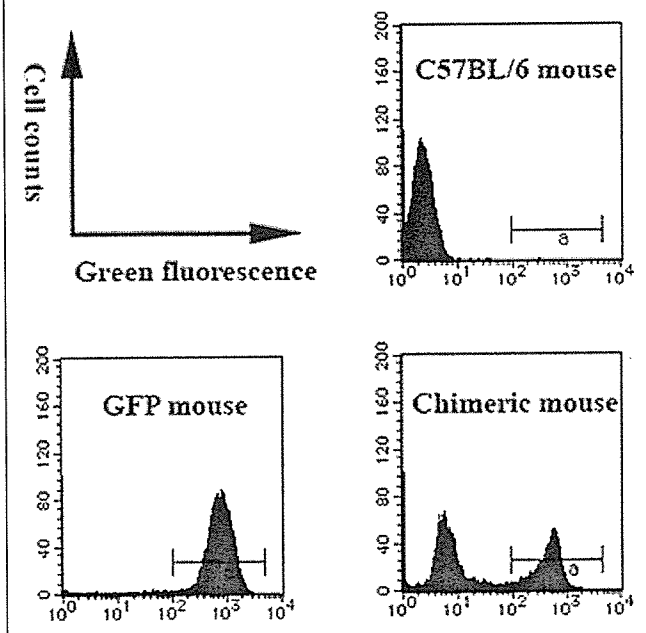

Migishima. Pregnancy after lethal dose irradiation. Fertil Steril 2006.

Table 2 summarizes the fecundity of the radiation-chimeric mice that were transplanted with fresh or frozen–thawed grafts examined after natural mating. Among five female mice that were exposed to 8.0 Gy radiation and transfused with mouse UCBCs without ovarian transplantation, pregnancy was not confirmed after mating with male B6C3F1 mice. However, in the group exposed to 8.0 Gy radiation that later were transfused with mouse UCBCs and transplanted with fresh ovarian grafts, four (80%) of five mice gave birth to a total of 14 pups that all were GFP positive. In the group exposed to 10.0 Gy radiation that later were transfused with mouse UCBCs and transplanted with fresh ovarian grafts, five (83.3%) of six mice gave birth to a total of 21 GFP positive pups. Similarly, in the group of mice exposed to 10.0 Gy of irradiation and that later were transfused with mouse UCBCs and transplanted with frozen–thawed ovarian grafts, three (60.0%) of five mice gave birth to a total of 12 GFP-positive pups.

Figure 3 shows the intraabdominal observation of pregnant mice (18 days of gestation from the day that the

FIGURE 2

Staining PBLs with antibodies to different lineage markers revealed that transfused cells had developed into T cells, B cells, Mac-1+ cells, granulocytes, and erythrocytes. Every lineage contained GFP+ cells.

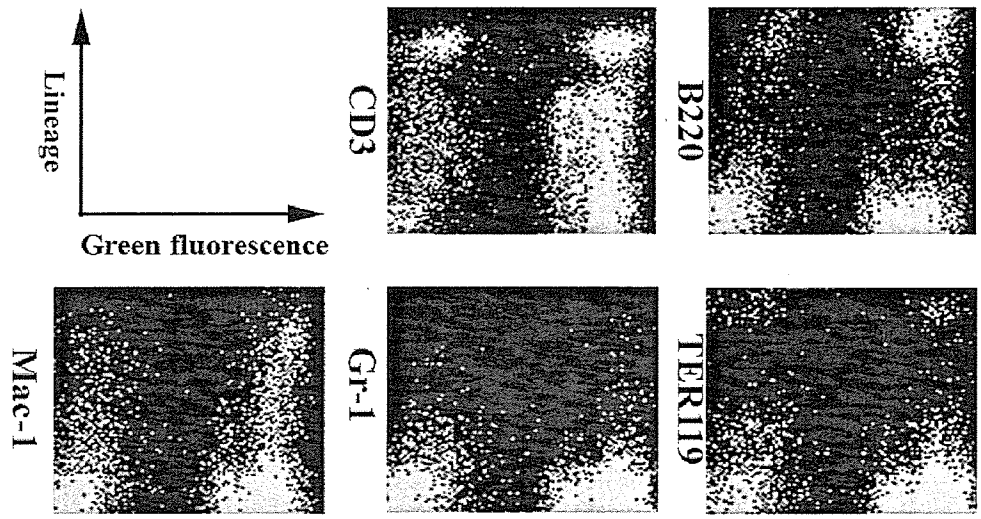

Migishima. Pregnancy after lethal dose irradiation. Fertil Steril 2006.

presence of a vaginal plug was confirmed) that were exposed to radiation and that later were transfused with UCBCs, had ovarian grafts transplanted, and were mated with male B6C3F1 mice.

Morphological Findings

Radiation-chimeric mice were killed 16 weeks after the transfusion of UCBCs. The ovaries were removed from the chimeric mice and embedded in the OCT compound. Frozen thin sections (8 μm thick) of the prepared ovaries were cut with a cryostat. The sections were stained with an anti-CD45 antibody and observed under a fluorescence microscope. In the lethally irradiated mice, no ovarian follicles were confirmed after histological evaluation. Many large cells were noted that appeared to be CD45-positive cells, which were noted to be macrophages by morphological findings (Fig. 4). We believe that after irradiation, these macrophages phagocytosed ovarian tissue cells and necrotic ovarian follicles. Although no ovarian follicles were noted in recipients that were exposed to lethal-dose irradiation, the ovarian tissues transplanted into these recipients had ovarian follicles histologically confirmed (Fig. 5).

DISCUSSION

Since the first successful clinical application of human umbilical cord blood transfusion by Gluckman et al. (10) in 1989, a number of clinical trials have proven the usefulness of UCBCs for reconstitution of the hematopoietic system (11, 12). Although the relatively slow engraftment is a drawback, transfusion of UCBCs has several advantages over bone marrow transfusion: the larger size of the available donor pool, enriched hematopoietic progenitor cells (13), low content of mature T cells causing graft-versus-host reaction (14, 15), and absence of cytomegalovirus infection

TABLE 1

Percentage of GFP+ cells in PBLs circulating in chimeric mice.

No. of recipients	Radiation dose (Gy)	Ovarian graft	Percentage of GFP+ cells of PBLs in chimeric mouse (mean ± SEM)
5	8	None	10.5 ± 2.9
5	8	Fresh	8.1 ± 1.7[a]
6	10	Fresh	34.6 ± 5.7
5	10	Frozen–thawed	46.9 ± 4.8[a]

[a] Significant difference ($P<.05$).

Migishima. Pregnancy after lethal dose irradiation. Fertil Steril 2006.

TABLE 2

Fecundity of radiation-chimeric mice transplanted with fresh or frozen–thawed ovarian grafts, examined after natural mating.

No. of recipients	Radiation dose (Gy)	Ovarian graft	No. (%) of recipients that gave birth to GFP+ pups	Total no. of pups born[a]	Pups born/ recipients (mean ± SEM)	Pups born/ one ovary (mean ± SEM)	Time before first delivery after mating (d) (mean ± SEM)
9	None	None	9 (100)	64	7.1 ± 1.5	3.6 ± 0.7	23.6 ± 3.7
5	8	None	0	0	0	0	—
5	8	Fresh	4 (80.0)	14	2.8 ± 0.3	2.8 ± 0.3	21.8 ± 0.2
6	10	Fresh	5 (83.3)	21	3.5 ± 0.7	3.5 ± 0.7	33.0 ± 2.2
5	10	Frozen-thawed	3 (60.0)	12	2.4 ± 0.5	2.4 ± 0.5	39.7 ± 5.1

[a] All of the pups born were GFP positive.

Migishima. Pregnancy after lethal dose irradiation. Fertil Steril 2006.

FIGURE 3

Abdominal cavity of 18.5-day-pregnant chimeric mouse that was transplanted with frozen–thawed ovaries. (**A**) Observation under visible light. (**B**) Observation when visible light and GFP excitation light are simultaneously used for illumination. F = fetus of GFP-transgenic mouse; L = lymph node of chimeric mouse (GFP fluorescence was observed in lymph node); O = transplanted frozen–thawed ovary from GFP-transgenic mouse (+/+); P = Peyer's patchlike tissue on colon, where GFP fluorescence was also observed; K = kidney; T = ovarian tube; U = part of the uterus. The GFP fluorescence was not observed in the kidney, ovarian tube, and uterus of the recipient.

Migishima. Pregnancy after lethal dose irradiation. Fertil Steril 2006.

(16). The number of umbilical cord blood transfusions performed has increased.

Recently, combination treatments including total body irradiation, cyclophosphamide, and other chemotherapeutic reagents have been used for pretreatment before hematopoi-

FIGURE 4

Histology of ovaries from lethally irradiated recipients that were transfused with GFP+ UCBCs. (**A**) Whole ovary from the radiation-chimeric mouse. Follicles were not observed in the ovarian tissue from irradiated mice. Cells that were GFP+ were noted sporadically in the ovary from the irradiated mouse. (**B**) Ovarian cortex from irradiated mouse. Follicles were not observed in the ovarian cortex from the irradiated mouse. (**C**) Medulla of the ovary from a chimeric mouse. Considerable large GFP+ cells were detected in panels **B** and **C.** (**D**) Merged images of considerable large GFP+ cells stained with anti-CD 45 antibody–labeled biotin and Texas red–labeled streptavidin. The GFP+ cells were considered to be macrophages by morphological findings. In every panel, bar = 100 μm.

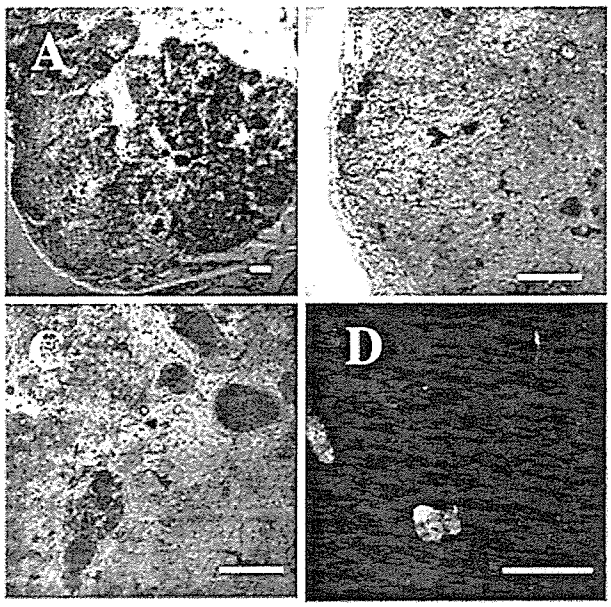

Migishima. Pregnancy after lethal dose irradiation. Fertil Steril 2006.

etic stem cell transfusion, including umbilical cord transfusion. It is known that administration of radiation and chemotherapeutic agents before transfusion of blood stem cells is harmful to gonadal function (1, 2). In prepubertal subjects with a history of bone marrow transfusion after radiation, menarche has been observed (16), the number of patients requiring estrogen or hormonal therapy to induce menses is increased (17), the rate of pregnancy in such patients is decreased (16, 18, 19), and decreased pituitary function has been noted (19), resulting in multiorgan dysfunction (20). The decreased pregnancy rate and requirement of hormonal therapy to induce menses most likely are a result of the decrease in or loss of ovarian follicles. Loss of follicular reserve and premature ovarian aging occur because primordial follicles are highly sensitive to cytotoxins (21, 22).

Although administration of radiation and chemotherapeutic reagents, such as busulfan and mitomycin C, has been used as pretreatment for hematopoietic stem cell transfusion in animal experiments, when hematopoietic stem cell transfusion experiments are performed, several days are required to allow hematopoietic stem cell engulfment after administration of chemotherapeutic agents, and it occasionally is not possible to transplant hematopoietic stem cells at the optimal time. For this reason, transfusion of hematopoietic stem cells after radiation rather than administration of chemotherapeutic agents commonly is performed to ensure hematopoietic stem cell engulfment.

With regard to the extent of injury to primordial follicles in ovaries by radiation, the dose at which half of the follicles in the ovaries from 8 weeks of age were lost (LD_{50}) was estimated to be 0.17 Gy (23). In humans, the estimated LD_{50} dose for follicle loss is 4 Gy (24).

However, it is difficult to generate radiation-chimeric mice with radiation at a dose of 4.0 Gy, necessitating the use of higher doses of radiation, because one of the purposes of our experiment was to confirm that umbilical cord blood stem cells derived from donors were functional in recipients. Therefore, during the process of production of radiation-chimeric mice, the function of ovaries of the chimeric mice might markedly have been diminished or already lost at the time of exposure to radiation at a dose of 8.0 Gy or 10.0 Gy. We generated chimeric mice with radiation at doses of 8.0 Gy and 10.0 Gy, but the ovarian follicles already had been lost, as shown in Figure 4. In addition, we verified that chimeric ratio in transfused umbilical cord blood of radiation-chimeric mice tended to increase and also demonstrated that it was indeed feasible to produce chimeric mice using umbilical cord blood stem cells via exposure to 8.0 Gy radiation. Moreover, the results of our experiment appeared to indicate that ovarian follicles in mouse ovaries were completely lost after whole-body radiation of mice at doses of ≥8.0 Gy. Furthermore, we performed GFP+ ovary transplantation, including that of frozen–thawed ovaries, and crossed the recipients with male B6C3F1 mice; all of the resulting offspring were positive for GFP. These in vivo data, together with the histological findings mentioned above, suggested that ovarian follicles in recipient mouse ovaries had been lost. Moreover, we transfused umbilical cord blood to mice exposed to 11.0 Gy radiation, but all mice died (data not shown).

Several clinical methods have been developed to avoid a hypogonadal state caused by chemotherapy or radiation. They include the freezing and storing of fertilized and unfertilized oocytes, as well as ovaries. Because fertilized oocytes or embryos are relatively stable during cryopreservation, this method is considered to be useful for maintaining fecundity. Cryopreservation of unfertilized oocytes has been applied clinically but still is experimental.

Preservation of frozen ovaries is still in an experimental stage at present. Several investigators have reported that

FIGURE 5

Stereomicroscopic findings with 480-nm blue light and with visible light of the recipients and donor. (**A–C**) Fresh ovarian grafts of GFP-transgenic mouse 4 months after transplantation. (**D–F**) Frozen–thawed ovarian grafts of GFP-transgenic mouse 4 months after transplantation. Note that the size of the fresh ovaries is generally larger than that of the frozen–thawed ovaries. (**A**, **D**) Findings with visible light. (**B**, **E**) Findings with 480-nm blue light. (**C**, **F**) Merged findings with 480-nm blue light and visible light. In every panel, bar = 200μm.

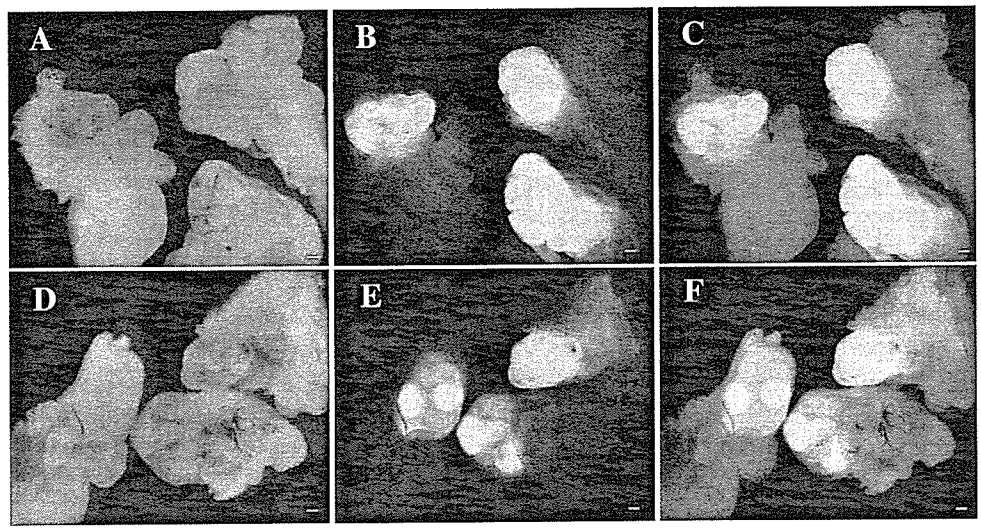

Migishima. Pregnancy after lethal dose irradiation. Fertil Steril 2006.

orthotopical implantation of cryopreserved ovarian tissues resulted in production of offspring. For example, Parrot (25), Gunasena et al. (26), and Sztein et al. (27) reported preservation of frozen ovaries in mice. In sheep, Gosden et al. (28) reported live births, whereas Salle et al. (29) reported birth of ewe, using slow-freezing techniques. Moreover a live birth after orthotopic transplantation of cryopreserved ovarian tissues in human has been reported (30, 31).

However, vitrification can avoid ice crystal formation during freezing and does not require a programmed freezer. Though vitrification has many advantages in cryobiology, only a few cases of offspring production have been reported with it thus far. In 2000, Takahashi et al. (32) reported live birth of mice, whereas Migishima et al. (6) reported live birth of mice in 2003 by vitrification. In 2005, Bordes et al. (33) reported live birth of a ewe. At present, only a few live births using vitrification methods have been reported, but in the near future, more cases of live births will be reported because of the ease of use of vitrification methods in preserving female fertility and because of improvement of techniques in vitrification methods and cryoprotectants.

Parrott and Parkes (3) reported in 1956 the maintenance of fecundity via ovarian transplantation to recipient mice with hypogonadism that was caused by exposure to radiation (16). This was the only report of ovarian transplantation using fresh ovaries after bone marrow transplantation. In our study, we produced radiation-chimeric mice using umbilical cord blood harvested from 18.5-day-old mice. In almost all experiments using umbilical cord blood transfusion, human umbilical cord blood was transfused into mice with severe combined immune deficiency and such; in other words, they were xenograft studies. In this case, compatibility between human factors, including hormones, and receptors in mice would be lowered by all means, or compatibility between some types of human factors and receptors in mice might be abolished. As a matter of fact, allografts usually are used in umbilical cord blood transfusion, if compared with animal experiments, thus necessitating performance of ovary transplantation experiments in the animal system, in compliance with umbilical cord blood transfusion that currently is being performed in human beings. In addition, because no investigators have conducted frozen–thawed ovary transplantation into chimeric mice, according to our literature search, we have performed frozen–thawed ovary transplantation experiments using chimeric mice.

In this study, the greatest attention was paid to [1] whether maintenance of fecundity is possible by transplantation of ovaries after recipients have been exposed to lethal-dose radiation and [2] whether transfusion of umbilical cord blood cells can maintain the potential for fecundity of recipients. Successful pregnancies were obtained after transplantation of frozen–thawed mouse ovaries into chimeric mice that had received lethal-dose radiation.

Previously, the decrease in or loss of fecundity caused by pretreatments such as irradiation chemotherapeutics was considered the price of treatment. However, our results in-

dicated that even with lethal radiation administered as pretreatment, the fecundity of recipients can be maintained if their ovaries are frozen and stored before they are exposed to radiation. Furthermore, it was demonstrated that blood stem cells from umbilical cord blood can save lethally irradiated recipients and have the potential to maintain the ability to achieve pregnancy in recipients with ovarian transplantation.

Acknowledgments: The authors thank Masaru Okabe, Ph.D., Osaka University, for donating GFP (+/+) mice and also thank Teresa K. Woodruff, Ph.D., Northwestern University, for giving valuable advice.

REFERENCES

1. Sanders JE, Buckner CD, Leonard JM, Sullivan KM, Witherspoon RP, Deeg HJ, et al. Late effects on gonadal function of cyclophosphamide, total-body irradiation, and marrow transplantation. Transplantation 1983;36:252–5.
2. Sanders JE, Pritchard S, Mahoney P, Amos D, Buckner CD, Witherspoon RP, et al. Growth and development following marrow transplantation. Blood 1986;68:1129–35.
3. Parrot DM, Parkes AS. Orthotopic ovarian grafting after sterilization by x-ray. Br Vet J 1956;112:550–4.
4. Migishima F, Suzuki-Migishima R, Song SY, Kuramochi T, Azuma S, Nishijima M, et al. Successful cryopreservation of mouse ovaries by vitrification. Biol Reprod 2003;68:881–7.
5. Okabe M, Ikawa M, Kominami K, Nakanishi T, Nishimura Y. "Green mice" as a source of ubiquitous green cells. FEBS Lett 1997;407: 313–9.
6. Migishima F, Oikawa A, Kondo S, Ema H, Morita Y, Nakauchi H, et al. Full reconstitution of hematopoietic system by murine umbilical cord blood. Transplantation 2003;75:1820–6.
7. Whitten WK, Biggers JD. Complete development in vitro of the preimplantation stages of the mouse in a simple chemically defined medium. J Reprod Fertil 1968;17:399–401.
8. Whittingham DG. Embryo banks in the future of developmental genetics. Genetics 1974;78:395–402.
9. Nakao K, Nakagata N, Katsuki M. Simple and efficient vitrification procedure for cryopreservation of mouse embryos. Exp Anim 1987;46: 231–4.
10. Gluckman E, Broxmeyer HA, Auerbach AD, Friedman HS, Douglas GW, Devergie A, et al. Hematopoietic reconstitution in a patient with Fanconi's anemia by means of umbilical cord blood from an HLA-identical sibling. N Engl J Med 1989;321:1174–8.
11. Gluckman E, Rocha V, Boyer-Chammard A, Locatelli F, Arcese W, Pasquini R, et al. Outcome of cord-blood transplantation from related and unrelated donors. Eurocord Transplant Group and the European Blood and Marrow Transplantation Group. N Engl J Med 1997;337: 373–8.
12. Rubinstein P, Carrier C, Scaradavou A, Kurtzberg J, Adamson J, Migliaccio AR, et al. Outcomes among 562 recipients of placental-blood transplants from unrelated donors. N Engl J Med 1998;339: 1565–77.
13. Wang JCY, Doedens M, Dick JE. Primitive human hematopoietic cells are enriched in cord blood compared with adult bone marrow or mobilized peripheral blood as measured by the quantitative in vivo SCID-repopulating cell assay. Blood 1997;89:3919–24.
14. Bofill M, Akbar A, Salmon M, Robinson M, Burford G, Janossy G. Immature CD45RA(low)RO(low) T cells in the human cord blood. I. Antecedents of CD45RA+ unprimed T cells. 1994;152:5613–23.
15. Madrigal JA, Cohen SB, Gluckman E, Charron DJ. Does cord blood transplantation result in lower graft-versus-host disease? It takes more than two to tango. Hum Immunol 1997;56:1–5.
16. Sanders JE. The impact of marrow transplant preparative regimens on subsequent growth and development. The Seattle Marrow Transplant Team. Semin Hematol 1991;28:244–9.
17. Salooja N, Szydlo RM, Socie G, Rio B, Chatterjee R, Ljungman P, et al; and Late Effects Working Party of the European Group for Blood and Marrow Transplantation. Pregnancy outcomes after peripheral blood or bone marrow transplantation: a retrospective survey. Lancet 2001;358:271–6.
18. Gulati SC, Van Poznak C. Pregnancy after bone marrow transplantation. J Clin Oncol 1998;16:1978–85.
19. Kauppila M, Koskinen P, Irjala K, Remes K, Viikari J. Long-term effects of allogeneic bone marrow transplantation (BMT) on pituitary, gonad, thyroid and adrenal function in adults. Bone Marrow Transplant 1998;22:331–7.
20. Sanders JE. Late effects in children receiving total body irradiation for bone marrow transplantation. Radiother Oncol 1990;18(Suppl 1):82–7.
21. Baker TG. Radiosensitivity of mammalian oocytes with particular reference to the human female. Am J Obstet Gynecol 1971;110:746–61.
22. Familiari G, Caggiati A, Nattola SA, Ermini M, Di Benedetto MR, Motta PM. Ultrastructure of human ovarian primordial follicles after combination chemotherapy for Hodgkin's disease. Hum Reprod 1993; 8:2080–7.
23. Gosden RG, Wade JC, Fraser HM, Sandow J, Faddy MJ. Impact of congenital or experimental hypogonadotrophism on the radiation sensitivity of mouse ovary. Hum Reprod 1997;12:2483–8.
24. Wallace WH, Shalet SM, Hendry JH, Morris-Jones PH, Gattamaneni HR. Ovarian failure following abdominal irradiation in childhood: the radiosensitivity of the human oocyte. Br J Radiol 1989;62:995–8.
25. Parrot DM. The fertility of mice with orthotopic ovarian grafts derived from frozen tissue. J Reprod Fertil 1960;1:230–41.
26. Gunasena KT, Villines PM, Crister ES, Crister JK. Live births after autologous transplant of cryopreserved mouse ovaries. Hum Reprod 1997;12:101–6.
27. Sztein J, Sweet H, Farley J, Mobraaten L. Cryopreservation and orthotopic transplantation of mouse ovaries: new approach in gamete banking. Biol Reprod 1998;58:1071–4.
28. Gosden RG, Baird DT, Wade JC, Webb R. Restoration of fertility to oophorectomized sheep by ovarian autografts stored at −196 degrees C. Hum Reprod 1994;9:597–603.
29. Salle B, Demirci B, Franck M, Rudigoz RC, Guerin JF, Lornage J. Normal pregnancies and live births after autograft of frozen-thawed hemi-ovaries into ewes. Fertil Steril 2002;77:403–8.
30. Donnez J, Dolmans MM, Demylle D, Jadoul P, Pirard C, Squifflet J, et al. Livebirth after orthotopic transplantation of cryopreserved ovarian tissue. Lancet 2004;364:1405–10.
31. Meirow D, Levron J, Eldar-Geva T, Harden I, Fridman E, Zalel Y, et al. Pregnancy after transplantation of cryopreserved ovarian tissue in a patient with ovarian failure after chemotherapy. N Engl J Med 2005;353:318–21.
32. Takahashi E, Miyoshi I, Nagasu T. Rescue of a transgenic mouse line by transplantation of a frozen-thawed ovaries obtained postmortem. Contemp Top Lab Anim Sci 2001;40:28–31.
33. Bordes A, Lornage J, Demirci B, Franck M, Courbiere B, Guerin JF, et al. Normal gestations and live births after orthotopic autograft of vitrified-warmed hemi-ovaries into ewes. Hum Reprod 2005;20: 2745–8.

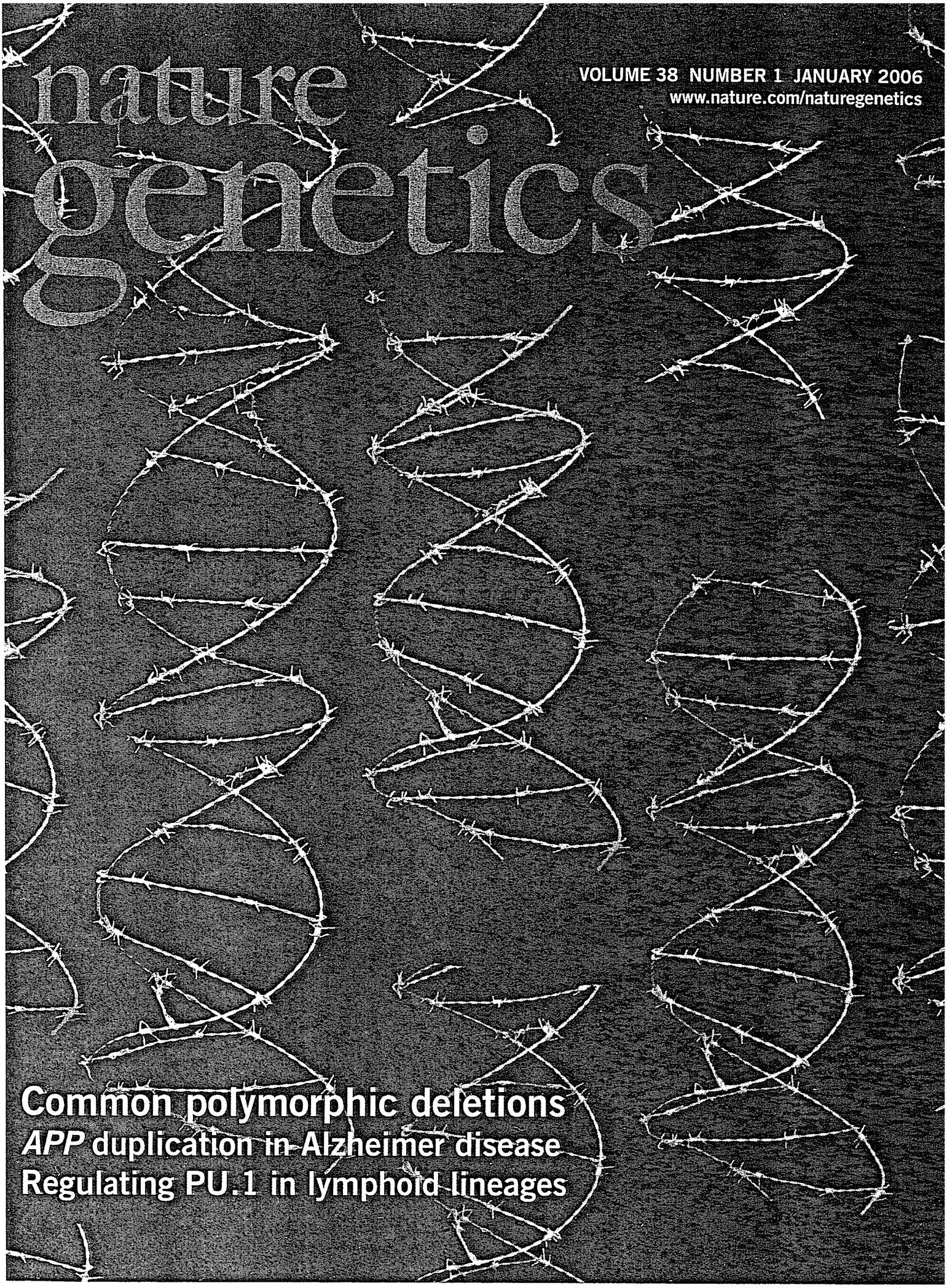
nature genetics
VOLUME 38 NUMBER 1 JANUARY 2006
www.nature.com/naturegenetics
Common polymorphic deletions
APP duplication in Alzheimer disease
Regulating PU.1 in lymphoid lineages

nature genetics

Deletion of *Peg10*, an imprinted gene acquired from a retrotransposon, causes early embryonic lethality

Ryuichi Ono[1,2], Kenji Nakamura[3], Kimiko Inoue[2,4], Mie Naruse[1], Takako Usami[5], Noriko Wakisaka-Saito[1,2,6,7], Toshiaki Hino[3], Rika Suzuki-Migishima[3], Narumi Ogonuki[4], Hiromi Miki[4], Takashi Kohda[1,2], Atsuo Ogura[2,4], Minesuke Yokoyama[2,3,8], Tomoko Kaneko-Ishino[2,7] & Fumitoshi Ishino[1,2]

By comparing mammalian genomes, we and others have identified actively transcribed Ty3/gypsy retrotransposon-derived genes with highly conserved DNA sequences and insertion sites[1–6]. To elucidate the functions of evolutionarily conserved retrotransposon-derived genes in mammalian development, we produced mice that lack one of these genes, *Peg10* (paternally expressed 10)[1–3,7], which is a paternally expressed imprinted gene on mouse proximal chromosome 6. The *Peg10* knockout mice showed early embryonic lethality owing to defects in the placenta. This indicates that *Peg10* is critical for mouse parthenogenetic development and provides the first direct evidence of an essential role of an evolutionarily conserved retrotransposon-derived gene in mammalian development.

Recently, we and others discovered the evolutionarily conserved retrotransposon-derived gene *Peg10* (refs. 1–3,8). Mouse *Peg10* is a single-copy gene located in an imprinted gene cluster on proximal chromosome 6, and its human homologue *PEG10* is in the syntenic imprinted region with identical gene order on human

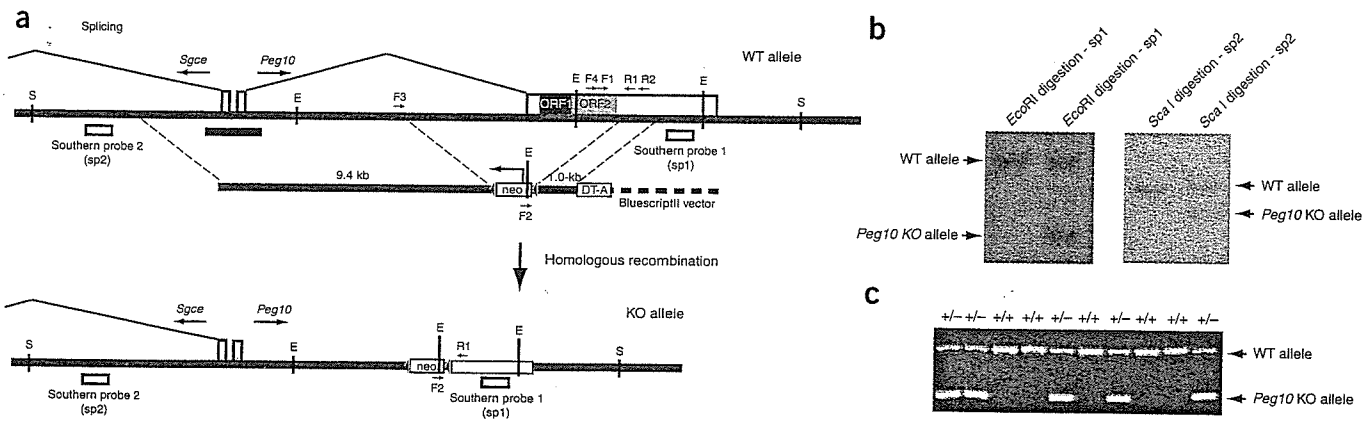

Figure 1 Targeted disruption of the *Peg10* locus. Schematic representation of the complete *Peg10* locus, the targeting vector and the targeted *Peg10* allele. Relevant restriction sites are indicated: E: *Eco*RI; S: *Sca*I. Primers are indicated by small arrows. (**a**) In the targeted allele, ORF1 and ORF2 were completely replaced by a neomycin resistance gene cassette. The *lox*P sites are shown as green triangles. WT, wild-type; KO: knockout. Black bar represents position of differentially methylated region (DMR). (**b**) DNA blot analysis of targeted ES cell clones. Genomic DNA was digested with *Eco*RI or *Sca*I and hybridized with Southern Probe 1 (SP1) or SP2. Left: wild-type ES cells; right: ES cells heterologous for the *Peg10* knockout allele. (**c**) Genotype analysis of 9.5-d.p.c. embryos by PCR using the *Peg10* F1, F2 and R1 primers. The results for each wild-type and Pat-KO embryo derived from mating a *Peg10* knockout chimera male with a wild-type female are shown.

[1]Department of Epigenetics, Medical Research Institute, Tokyo Medical and Dental University, 2-3-10 Kandasurugadai, Chiyoda-ku, Tokyo 101-0062, Japan. [2]CREST, Japan Science and Technology Agency (JST), 4-1-8 Hon-machi, Kawaguchi, Saitama 332-0011, Japan. [3]Mitsubishi Kagaku Institute of Life Sciences, 11 Minamiooya, Machida, Tokyo 194-8511, Japan. [4]BioResource Center, RIKEN, 3-1-1 Koyadai, Tsukuba, Ibaraki 305-0074, Japan. [5]Facility for Recombinant Mice, Medical Research Institute, Tokyo Medical and Dental University, 2-3-10 Kandasurugadai, Chiyoda-ku, Tokyo 101-0062, Japan. [6]Division for Gene Research, Center for Biological Resources and Informatics, Tokyo Institute of Technology, 4259 Nagatsuta-cho, Midori-ku, Yokohama 226-8501, Japan. [7]School of Health Sciences, Tokai University, Bohseidai, Isehara, Kanagawa 259-1193, Japan. [8]Present address: Brain Research Institute, Niigata University, 1-757 Asahimachi-dori, Niigata 951-8585, Japan. Correspondence should be addressed to T.K.-I. (tkanekoi@is.icc.u-tokai.ac.jp) or F.I. (fishino.epgn@mri.tmd.ac.jp).

Received 2 February; accepted 4 October; published online 11 December 2005; doi:10.1038/ng1699

Table 1 Lethality of *Peg10* knockout (Pat-KO) fetuses and neonates

Dissection stage (d.p.c.)	*Peg10*$^{+/+}$ total	Pat-KO total (dead)	Percentage death in Pat-KO
Embryos from male chimeras			
8.5	9	13 (0)	0
9.5	12	12 (0)	0
10.5	8	4[a] (4)	100
11.5–12.5	2	2 (2)	100
12.5–term	3	12 (12)	100
Born	53	0 (nd)	100
Embryos from F2 males			
8.5	14	5 (0)	0
9.5	37	35 (0)	0
10.5	12	10[a] (10)	100
11.5–12.5	13	17 (17)	100
12.5–term	12	10 (10)	100
Born	16	0 (nd)	100

No *Peg10* Pat-KO pups were born as the result of natural mating of two male chimeras and three F2 males with normal C57BL/6 females. *In utero*, viable Pat-KO embryos were present in numbers consistent with normal mendelian inheritance before 9.5 d.p.c. However, all of these embryos died until 10.5 d.p.c. nd, not detected.
[a]Embryos that died before 10.5 d.p.c. were severely growth retarded and apparently dead, as no heartbeat was detectable and their bodies were resorbed.

chromosome 7q21. Structural analysis of *Peg10* clearly showed that it was derived from a Ty3/gypsy long terminal repeat (LTR) retrotransposon, as is the Sushi-ichi retrotransposon[9] (with which it shows most similarity), but it does not function as an active retrotransposon. It is expressed in some embryonic tissues and extensively in the placenta as an endogenous gene[1,8]. Notably, *Peg10* is highly conserved across mammalian species. As far as we know, *Peg10* orthologues are present in all mammals, suggesting that it acquired some essential function as an endogenous gene after losing its transposition capabilities[1,8].

We attempted to generate *Peg10* knockout mice to explore this hypothesis. As we first isolated *Peg10* as a candidate imprinted gene for an early embryonic lethal phenotype of mice with maternal duplication of proximal chromosome 6 (ref. 10), it is possible that *Peg10* knockout mice might show parent of origin–specific lethality. A targeting vector was designed to remove the entire coding regions of ORF1 and ORF2 while retaining the promoter region, as it overlaps a differentially methylated region (DMR; **Fig. 1a**). Using targeted embryonic stem (ES) cell clones (**Fig. 1b**), we produced two male chimeric mice whose progeny inherited recombinant ES cell–derived alleles at a very high rate. However, none of the pups had the knockout alleles (**Table 1**). We dissected pregnant females at various embryonic stages and found that all *Peg10*$^{+/-}$ embryos died *in utero* by 10.5 d post coitus (d.p.c.; **Table 1** and **Fig. 1c**), although they were detected at approximately the expected mendelian frequency before 9.5 d.p.c. (**Table 1**).

Morphologically, the *Peg10*$^{+/-}$ embryos and yolk sacs appeared normal at 9.5 d.p.c. as they reached the major development steps, such as functional chorioallantoic fusion, rotation, formation of head structures, initiation of cardiac contraction and vascularization of the yolk sac (**Fig. 2a,b**). However, they became severely growth retarded and had no detectable heartbeat at 10.5 d.p.c. (**Fig. 2c,d**). Their placentas were slightly smaller than those of the normal wild-type at 9.5 d.p.c. and became severely depleted at 10.5 d.p.c. The labyrinth layer was not developed and no spongiotrophoblast cells were observed at 9.5–10.5 d.p.c. (**Fig. 2e–h**). However, there were no

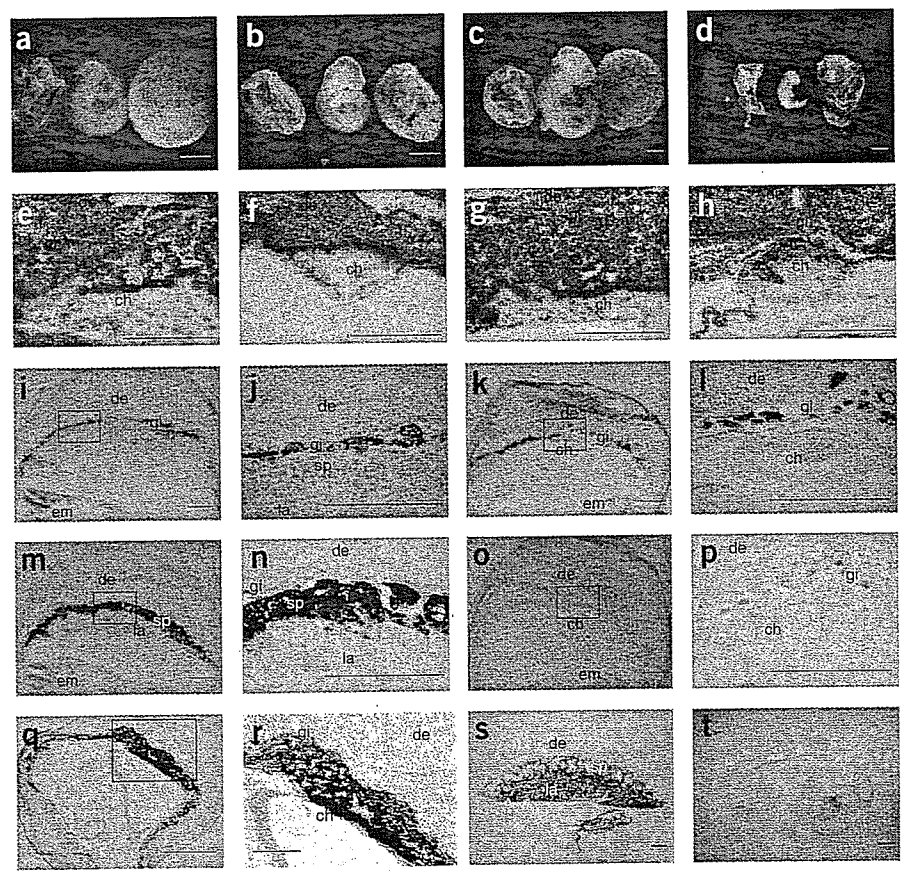

Figure 2 *Peg10* knockout embryos show severe growth retardation and placental defects. Wild-type (**a,c**) and Pat-KO (**b,d**) embryos (em) are shown, together with their placentas (right) and yolk sacs (left) at 9.5 d.p.c. (**a,b**) and 10.5 d.p.c. (**c,d**) (scale bars: 1 mm). The Pat-KO embryos have poorly developed placentas. Hematoxylin and eosin–stained histological sections of 9.5-d.p.c. (**e,f**) and 10.5-d.p.c. (**g,h**) wild-type (**e,g**) and Pat-KO (**f,h**) littermates (scale bars: 500 μm). The trophoblast giant cells (gi), spongiotrophoblast (sp), labyrinthine (la), chorionic plate (ch) and maternal decidua (de) are normal in the wild-type placentas, whereas poorly developed placentas are observed in the Pat-KO mice. The *in situ* hybridization of 10.5-d.p.c. wild-type (**i,j,m,n**) and Pat-KO (**k,l,o,p**; scale bars: 500 μm) using the trophoblast-specific marker gene *PL-1* (**i-l**) for trophoblast giant cells and the *4311* probe (**m–p**) for spongiotrophoblast cells, clearly demonstrates that the giant cells are normal, whereas the spongiotrophoblast cells, which are derived from the ectoplacental cone, are completely missing (**o,p**). Higher magnifications of the boxed regions of **i,k,m,o** are shown as **j,l,n,p**, respectively. *In situ* hybridization with the antisense *Peg10* probe of the wild-type conceptus at 9.5 d.p.c. (**q**; scale bar: 500 μm) and 12.5 d.p.c. placenta (**s**) and embryo (**t**; scale bar, 1 mm) demonstrates that *Peg10* is strongly expressed in all the extraembryonic tissues at these stages (**q,s**), and relatively well expressed in the brain and vertebral cartilage (**t**). (**r**) Higher magnifications of the boxed regions shown in **q** (scale bar: 200 μm).

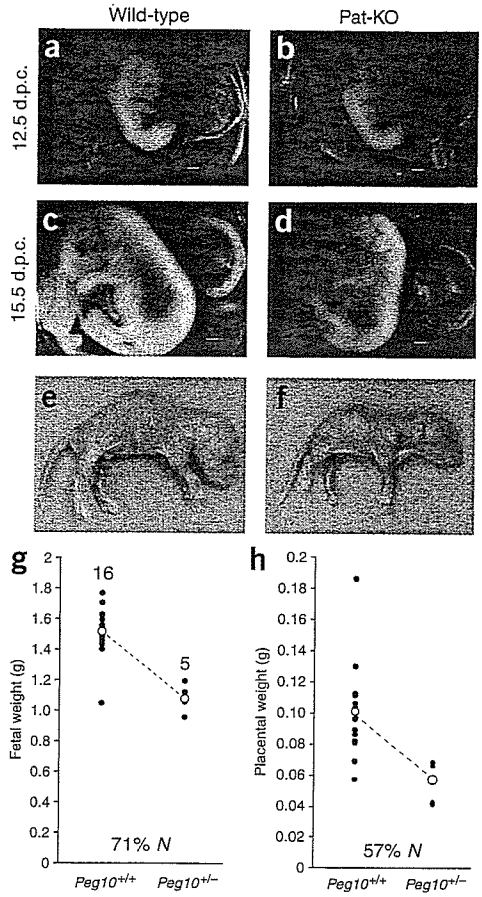

Figure 3 Rescue of *Peg10* Pat-KO embryos by tetraploid wild-type extraembryonic tissues. Wild-type and Pat-KO embryos with their placentas (right) and yolk sacs (left) rescued by tetraploid wild-type extraembryonic tissues. Weights in **a**,**b** are as follows (mean ± s.d.): $Peg10^{+/+}$ embryo, 0.092 ± 0.003 ($n = 2$); $Peg10^{+/-}$ embryo, 0.091 ($n = 1$); $Peg10^{+/+}$ placenta, 0.051 ± 0.005 ($n = 2$); $Peg10^{+/-}$ placenta, 0.057 ($n = 1$). Weights in **c**,**d** are as follows: $Peg10^{+/+}$ embryo, 0.548 ± 0.065 ($n = 3$), $Peg10^{+/-}$ embryo, 0.411 ± 0.027 ($n = 3$), $P = 0.028$; $Peg10^{+/+}$ placenta, 0.113 ± 0.003 ($n = 3$); $Peg10^{+/-}$ placenta, 0.122 ± 0.005 ($n = 3$), $P = 0.049$). Scale bar: 1 mm. (**e**,**f**) Wild-type and Pat-KO newborn pups rescued by tetraploid wild-type extraembryonic tissues (scale bars: 1 mm). (**g**) Fetal weights of *Peg10* Pat-KO and wild-type littermates rescued by tetraploid wild-type extraembryonic tissues at 19.5 d.p.c. Each filled circle represents a single embryo. Number at top represents total number of weighed embryos. Open circles represent average weight. The degree of growth deficiency of the rescued Pat-KO embryos is shown as a percentage of wild-type fetal weight (*N*). Fetal weights (mean ± s.d.) are as follows: $Peg10^{+/+}$, 1.526 ± 0.159 ($n = 16$); $Peg10^{+/-}$, 1.089 ± 0.088 ($n = 5$); $P = 1.306 \times 10^{-55}$. (**h**) Placental weights of *Peg10* Pat-KO and wild-type littermates rescued by tetraploid wild-type extraembryonic tissues at 19.5 d.p.c. The data are from the same litters as in **g**. Placental weights (mean ± s.d.) are as follows: $Peg10^{+/+}$, 0.102 ± 0.029 ($n = 16$); $Peg10^{+/-}$, 0.058 ± 0.014 ($n = 5$); $P = 0.004$.

morphological differences in the placentas at 7.5 d.p.c. and 8.5 d.p.c. (**Supplementary Fig. 1** online). *In situ* hybridization of 8.5- to 10.5-d.p.c. placentas with trophoblast-specific marker genes (*PL-1* for trophoblast giant cells and *Tpbpa* for spongiotrophoblast cells) clearly demonstrated that although the giant cells were normal (**Fig. 2i–l** and **Supplementary Fig. 1**), the spongiotrophoblast cells, which are derived from the ectoplacental cone, were completely missing (**Fig. 2m–p** and **Supplementary Fig. 1**). Therefore, we conclude that these placentas are abnormal compared with typical three-layered placentas. In light of these defects, it is conceivable that the severe defect in placenta formation was the cause of the growth retardation and early embryonic lethality of the $Peg10^{+/-}$ embryos. The *Peg10* expression profile supports this assumption: high expression in all the extraembryonic tissues at 9.5 d.p.c. and 12.5 d.p.c. (**Fig. 2q–s**)[1,8] and low-level expression in the embryonic brain and vertebral cartilage at 12.5 d.p.c. (**Fig. 2t**).

To confirm these findings, we attempted to rescue the phenotype by aggregating $Peg10^{+/-}$ embryos with tetraploid embryos derived from wild-type fertilized eggs[11]. As expected, 12.5- and 15.5-d.p.c. knockout embryos were recovered with normal-looking placentas, although the latter showed growth retardation in both embryos and placentas (**Fig. 3a–d**). As a result, half of the knockout embryos (18/37) developed to term, demonstrating that the early embryonic lethality of $Peg10^{+/-}$ results from incomplete placenta formation (**Fig. 3e,f**). Recovered $Peg10^{+/-}$ embryos showed growth retardation in most cases (**Fig. 3g,h**). However, the fetal-to-placental weight ratios of $Peg10^{+/-}$ embryos were slightly higher than those of the wild-type embryos, suggesting the mutant placenta, although small, is relatively more efficient than the wild-type placenta (**Supplementary Fig. 2** online).

Although the *Peg10* knockout mice had approximately 30% lower weight at birth than their wild-type littermates (**Fig. 3g**), they gained weight, and the *Peg10* knockout F_1 females delivered F_2 pups normally with or without the knockout allele (Mat-KO; **Fig. 4a**). These F_2 pups matured normally, *Peg10* knockout F_2 females consistently had normal deliveries, and F_3 pups with the knockout allele grew normally. Conversely, all the F_3 embryos with the knockout allele died by 10.5 d.p.c. in paternal transmission (Pat-KO; **Table 1** and **Fig. 4a**).

Quantitative RT-PCR of the entire region showed normal expression of fifteen genes, which included at least six imprinted genes, in 9.5-d.p.c. Pat-KO embryos, whereas *Peg10* itself was not expressed (**Fig. 4b**). We also confirmed that the differential DNA methylation status of the *Peg10-Sgce* DMR remained normal[8], using polymorphisms between JF1 (*Mus musculus molossinus*) and *Mus musculus musculus* (**Fig. 4c**). The early embryonic lethal phenotype was also observed in this genetic background (data not shown). The expression of *Ppp1r9a* (*Neurabin*) was apparently reduced in affected 9.5- and 10.5-d.p.c. Pat-KO placentas (**Fig. 5**) but normal in the normal-looking 8.5-d.p.c. Pat-KO placentas, which suggests that the *Peg10* knockout does not affect the expression levels of nearby placental genes (**Fig. 5**). All the basic phenotypes of the *Peg10* knockout embryos were confirmed in *Peg10 lox*P knockout mice without a *neo* expression cassette (**Supplementary Figs. 3–5** and **Supplementary Table 1** online). Thus, we conclude that *Peg10* is essential for placenta formation and is responsible for the early embryonic lethality seen during mouse development. Our results also suggest that *Peg10* is one of the lethal target genes in mice with maternal duplication of proximal chromosome 6, which bears the *Peg10* locus[10].

Deletion of the maternally expressed imprinted gene *Ascl2* (also known as *Mash2*)[12] leads to early embryonic lethality (death by 10.5 d.p.c.) owing to similar placental morphological defects to *Peg10* Pat-KO embryos. Therefore, we examined the expression of *Ascl2* in *Peg10* knockout embryos using quantitative RT-PCR (**Supplementary Fig. 6**) and found that *Ascl2* expression was normal at 8.5 d.p.c. but heavily reduced at 9.5 d.p.c., probably owing to a lack of spongiotrophoblasts and labyrinth cells. These results clearly indicate that *Peg10* is not situated upstream of *Ascl2*.

Our present study also indicates that *Peg10* could be critical for parthenogenetic development in mice because parthenogenetic

embryos that contain two maternally derived genomes lack expression of all paternally expressed imprinted genes. Parthenogenetic embryos die before 9.5 d.p.c. and show early embryonic lethality with poorly developed extraembryonic tissues[13,14]. Morphological defects of the most developed parthenotes are very similar to those of *Peg10*-Pat KO embryos; they lack the diploid trophoblast cells of the labyrinth layer and the spongiotrophoblast but have some giant cells and some chorion at days 9 and 10 (ref. 15). However, the majority of parthenotes show more severe phenotypes; the diploid trophoblast cells of the ectoplacental cone almost completely fail to develop, leading to lack of extraembryonic ectoderm, and therefore chorion, so that at 6.5 d.p.c. the conceptus is abnormal, despite the vigorous embryonic ectoderm (S. Barton and M.A. Surani, personal communication). Therefore, it is clear that some other genes could also contribute to the parthenogenetic phenotypes[13,14].

The genetic conflict hypothesis predicts that genes that promote embryonic and placental growth have become paternally expressed,

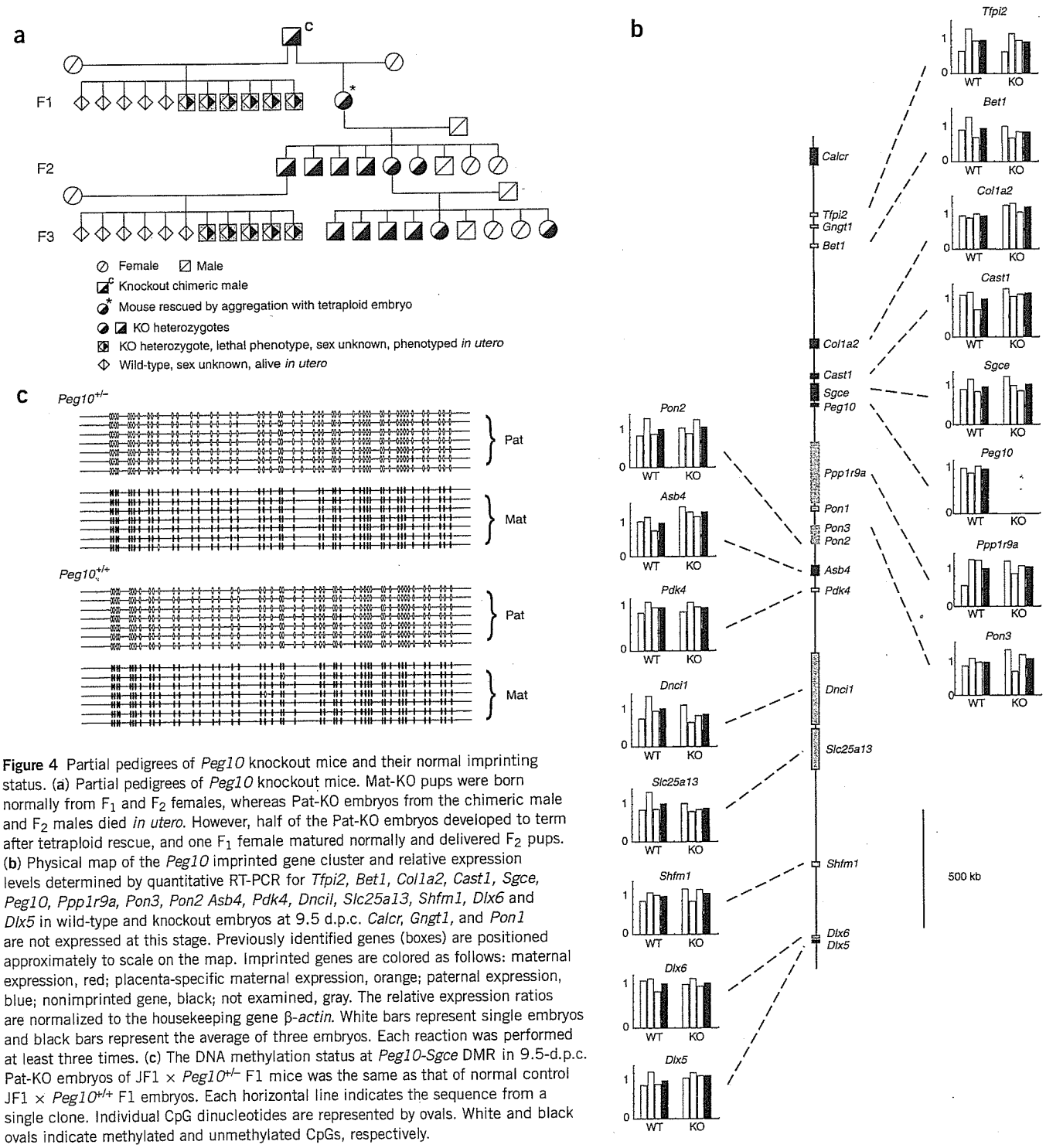

Figure 4 Partial pedigrees of *Peg10* knockout mice and their normal imprinting status. (**a**) Partial pedigrees of *Peg10* knockout mice. Mat-KO pups were born normally from F_1 and F_2 females, whereas Pat-KO embryos from the chimeric male and F_2 males died *in utero*. However, half of the Pat-KO embryos developed to term after tetraploid rescue, and one F_1 female matured normally and delivered F_2 pups. (**b**) Physical map of the *Peg10* imprinted gene cluster and relative expression levels determined by quantitative RT-PCR for *Tfpi2, Bet1, Col1a2, Cast1, Sgce, Peg10, Ppp1r9a, Pon3, Pon2 Asb4, Pdk4, Dncil, Slc25a13, Shfm1, Dlx6* and *Dlx5* in wild-type and knockout embryos at 9.5 d.p.c. *Calcr, Gngt1,* and *Pon1* are not expressed at this stage. Previously identified genes (boxes) are positioned approximately to scale on the map. Imprinted genes are colored as follows: maternal expression, red; placenta-specific maternal expression, orange; paternal expression, blue; nonimprinted gene, black; not examined, gray. The relative expression ratios are normalized to the housekeeping gene β-*actin*. White bars represent single embryos and black bars represent the average of three embryos. Each reaction was performed at least three times. (**c**) The DNA methylation status at *Peg10-Sgce* DMR in 9.5-d.p.c. Pat-KO embryos of JF1 × *Peg10*$^{+/-}$ F1 mice was the same as that of normal control JF1 × *Peg10*$^{+/+}$ F1 embryos. Each horizontal line indicates the sequence from a single clone. Individual CpG dinucleotides are represented by ovals. White and black ovals indicate methylated and unmethylated CpGs, respectively.